UPPSALA
UNIVERSITET

Digital Comprehensive Summaries of Uppsala Dissertations from the Faculty of Science and Technology 280

Advanced Thin Film Electroacoustic Devices

JOHAN BJURSTRÖM

ACTA
UNIVERSITATIS
UPSALIENSIS
UPPSALA
2007

ISSN 1651-6214
ISBN 978-91-554-6819-4
urn:nbn:se:uu:diva-7672

Dissertation presented at Uppsala University to be publicly examined in Polhemssalen, Ångströmlaboratoriet, Lägerhyddsvägen 1, Uppsala, Friday, March 30, 2007 at 09:30 for the degree of Doctor of Philosophy. The examination will be conducted in English.

Abstract

Bjurström, J. 2007. Advanced Thin Film Electroacoustic Devices. (Avancerade Elektroakustiska Tunnfilmskomponenter). Acta Universitatis Upsaliensis. *Digital Comprehensive Summaries of Uppsala Dissertations from the Faculty of Science and Technology* 280. 84 pp. Uppsala. ISBN 978-91-554-6819-4.

The explosive development of the telecom industry and in particular wireless and mobile communications in recent years has lead to a rapid development of new component and fabrication technologies to continually satisfy the mutually exclusive requirements for better performance and miniaturization on the one hand and low cost on the other. A fundamental element in radio communications is time and frequency control, which in turn is achieved by high performance electro-acoustic components made on piezoelectric single crystalline substrates. The latter, however, reach their practical limits in terms of performance and cost as the frequency of operation reaches the microwave range. Thus, the thin film electro-acoustic technology, which uses thin piezoelectric films instead, has been recently developed to alleviate these deficiencies.

This thesis explores and addresses a number of issues related to thin film synthesis on the one hand as well as component design and fabrication on other. Specifically, the growth of highly c-axis textured AlN thin films has been studied and optimized for achieving high device performance. Perhaps, one of the biggest achievements of the work is the development of a unique process for the deposition of AlN films with a mean c-axis tilt, which is of vital importance for the fabrication of resonators operating in contact with liquids, i.e. biochemical sensors. This opens the way for the development of a whole range of sensors and bio-analytical tools. Further, high frequency Lamb wave resonators have been designed, fabricated and evaluated. Performance enhancement of FBAR devices is also addressed, e.g. spurious mode suppression, temperature compensation, etc. It has been demonstrated, that even without temperature compensation, shear mode resonators operating in a liquid still exhibit an excellent performance in terms of Q (200) and coupling (~1.8%) at 1.2 GHz, resulting in a mass resolution better than 2 ng cm^{-2} in water, which excels that of today's quartz sensors.

Keywords: aluminum nitride, FBAR, shear mode resonator, lamb wave devices, liquid sensor, biosensor, temperature compensation, reactive sputtering

Johan Bjurström, Department of Engineering Sciences, Box 534, Uppsala University, SE-75121 Uppsala, Sweden

ISSN 1651-6214
ISBN 978-91-554-6819-4
urn:nbn:se:uu:diva-7672 (http://urn.kb.se/resolve?urn=urn:nbn:se:uu:diva-7672)

In memory of
My
Wife Paulina and Mother Inger

List of Appended Papers

I J. Bjurström, L. Vestling, J. Olsson, and I. Katardjiev, "An accurate direct extraction technique for the MBVD resonator model," *Proceedings of the 34th European Microwave Conference,* Amsterdam*,* 2004.

II D. Rosen, J. Bjurström, and I. Katardjiev, "Suppression of spurious lateral modes in thickness-excited FBAR resonators," *IEEE Transactions on Ultrasonics,Ferroelectrics and Frequency Control*, vol. 52, pp. 1189-1192, 2005.

III G. F. Iriarte, J. Bjurström, J. Westlinder, F. Engelmark, and I. V. Katardjiev, "Synthesis of c-axis-oriented AlN thin films on high-conducting layers: Al, Mo, Ti, TiN, and Ni," *IEEE Transactions on Ultrasonics, Ferroelectrics and Frequency Control*, vol. 52, pp. 1170-1174, 2005.

IV J. Bjurström, D. Rosen, I. Katardjiev, V. M. Yanchev, and I. Petrov, "Dependence of the electromechanical coupling on the degree of orientation of c-textured thin AlN films," *IEEE Transactions on Ultrasonics, Ferroelectrics and Frequency Control*, vol. 51, pp. 1347-1353, 2004.

V J. Bjurström, G. Wingqvist, and I. Katardjiev, "Synthesis of textured thin piezoelectric AlN films with a nonzero C-axis mean tilt for the fabrication of shear mode resonators," *IEEE Transactions on Ultrasonics, Ferroelectrics and Frequency Control*, vol. 53, pp. 2095-2100, 2006.

VI J. Bjurström, I. Katardjiev, and V. Yantchev, "Lateral-field-excited thin-film Lamb wave resonator," *Applied Physics Letters*, vol. 86, pp. 154103, 2005.

VII J. Bjurström, V. Yantchev, and I. Katardjiev, "Thin film Lamb wave resonant structures - The first approach," *Solid-State Electronics*, vol. 50, pp. 322-326, 2006.

VIII G. Wingqvist, J. Bjurström, L. Liljeholm, V. Yantchev, and I. Katardjiev, "Shear mode AlN thin film electro-acoustic resonant sensor operation in viscous media," *Sensors and Actuators B: Chemical*, vol. In Press, Corrected Proof.

IX J. Bjurström, G. Wingqvist, V. Yantchev, and I. Katardjiev, "Temperature compensation of liquid FBAR sensors," *Journal of Micromechanics and Microengineering*, vol. 17, pp. 651-658, 2007.

Conference Contributions and Related Papers

i. G. F. Iriarte, J. Bjurström, J. Westlinder, F. Engelmark, and I. V. Katardjiev, "Synthesis of c-axis oriented AlN thin films on metal layers: Al, Mo, Ti, TiN and Ni," presented at IEEE Ultrasonics Symposium, Munich, Germany, 2002.

ii. J. Bjurström, D. Rosén, I. Katardjiev, and V. Yanchev, "Dependence of the Electromechanical Coupling on the Degree of Orientation of c-Textured Thin AlN Films," presented at IEEE Ultrasonics Symposium, Honolulu, Hawaii, USA, 2003.

iii. D. Rosen, J. Bjurström, I. Katardjiev, and F. Engelmark, "Suppression of Spurious Lateral Modes in Thickness Excited FBAR Resonators," presented at IEEE Ultrasonics Symposium, Honolulu, Hawaii, USA, 2003.

iv. J. Bjurström, G. Wingqvist, and I. Katardjiev, "Synthesis of textured thin piezoelectric AlN films with a nonzero c-axis mean tilt for the fabrication of shear mode resonators," presented at IEEE Ultrasonics Symposium, Rotterdam, Netherlands, 2005.

v. G. Wingqvist, J. Bjurström, L. Liljeholm, I. Katardjiev, and A. L. Spetz, "Shear mode AlN thin film electroacoustic resonator for biosensor applications," presented at IEEE Sensors, Irvine, Ca, USA, 2005.

vi. J. Bjurström, G. Wingqvist, V. Yantchev, and I. Katardjiev, "Design and fabrication of temperature compensated liquid FBAR sensors," presented at IEEE Ultrasonics Symposium, Vancouver, Canada, 2006.

vii. V. Yantchev, J. Enlund, J. Bjurström, and I. Katardjiev, "Design of high frequency piezoelectric resonators utilizing laterally propagating fast modes in thin aluminum nitride (AlN) films," Ultrasonics, vol. 45, pp. 208-212, 2006.

viii. G. Wingqvist, J. Bjurström, A.-C. Hellgren, and I. Katardjiev, "Immunosensor utilizing Shear mode thin film bulk acoustic sensor," presented at 20th Anniversary Eurosensors Göteborg, Sweden, 2006.

Patent application

I. Katardjiev, J. Bjurström, and G. Wingqvist, "Production of polycrystalline films for shear mode piezoelectric thin film resonators," International patent application PCT/SE2006/050041, 2006.

Contents

1 Introduction

The explosive development of the telecommunication industry and in particular wireless and mobile communications in recent years has lead to the rapid development of new components and fabrication technologies to continually satisfy the mutually exclusive requirements for better performance and miniaturization on the one hand and low cost on the other. A fundamental element in radio communications is time and frequency control, which in turn is achieved by high performance electro-acoustic components made on piezoelectric substrates (quartz, LiNbO3, etc). The latter, however, reach their practical limits in terms of performance and cost as the frequency of operation reaches the microwave range. Thus, the thin film electroacoustic (TEA) technology, which uses thin piezoelectric films instead, has been recently developed to alleviate these deficiencies. Perhaps, one of the biggest potentials of the TEA technology is that it opens the very promising possibility of integrating the traditionally incompatible IC and electro-acoustic technologies. Another very significant benefit from this integration would be the mass fabrication of highly sensitive, low cost integrated chemical and biological sensors and electronic tags. Environmental control is becoming of great importance for today's society both for the manufacturing industry and public sectors. The increasing threat of chemical and biological sabotage along with that of hazardous industrial incidents necessitate large scale monitoring of the environment which can only be done by mass produced low cost sensors.

This thesis explores various aspects of the TEA technology and addresses a number of issues related to thin film synthesis on the one hand as well as component design and fabrication on other.

1.1 Electroacoustic devices – A survey

One of the key events leading directly to the emergence of electro-acoustic (EA) devices was the discovery of piezoelectricity by the Curie brothers in 1880. It first found practical use in World War I, which led to the introduction of quartz transducers when Langevin in 1915 utilized a (steel-quartz-steel) bulk acoustic wave (BAW) transducer in pulse echo experiments at high frequencies (150 kHz) for object detection in water. His work was followed up by Cady, which led to the development of crystal-

controlled oscillators based on quartz [1]. Later in the second half of the 20th century the quartz crystal microbalance (QCM) became a widely used sensor for the detection of mass loading from atomic and molecular species in gaseous and aqueous media. Quartz has been and still is of primary importance in signal processing and sensor applications due to superior properties such as low acoustic losses and excellent temperature stability.

Extensive work in the ultrasonic field done by Lord Rayleigh in the 20th century resulted in the discovery of surface acoustic (Rayleigh) waves (SAW), although it remained for quite some time a scientific curiosity with very few applications. The development of the interdigital transducer (IDT) by White and Voltmer in the 1960s led to a breakthrough in the SAW device technology, which allowed the use of process techniques, originally developed for microelectronics, in the fabrication of high frequency SAW devices in large quantities. One of the earliest SAW application was an intermediate frequency (IF) bandpass filter for television receivers developed in the 1970s [2]. Typical substrate materials for these devices are quartz and expensive but very high-performance refractory oxides such as single crystalline lithium niobate ($LiNbO_3$) and lithium tantalate ($LiTaO_3$).

Before 1980 the major investments in research and development of micro wave acoustics was for military as well as professional communication and radar systems. Today, the majority of electro-acoustic wave devices can be found in a wide range of consumer applications such, TV, radio, mobile phone communications, wireless ID tags, sensors, etc. The telecom industry alone consumes annually nearly four billion SAW based radio frequency (RF) bandpass filters primarily for mobile phones and base-stations [2]. Other applications for RF filters are GPS, navigation systems, base stations for mobile phone systems, and relatively new systems for wireless data transfer (Bluetooth, WLAN) [3]. The frequency of operation for the above applications lies typically in the range 400 MHz to 6 GHz, where conventional LC filters suffer from unacceptable losses. Electromagnetic filters based on ceramic materials exhibit low losses and a good power handling capability but are on the other hand very large and therefore impractical for applications where a high level of miniaturization is required. SAW filters based on bulk single crystalline piezoelectric materials dominate the filter market today for frequencies up to 3 GHz [2] mainly due to their small size, low cost and simplicity of fabrication.

One of the biggest disadvantages using single-crystalline substrates in BAW and SAW devices is that the choice of piezoelectric materials is rather limited and which materials in addition are incompatible with the IC technology. Further, the properties of these materials determine uniquely the acoustic velocity, which in turn together with the device dimensions define the operating frequency. High frequency QCM operation for instance, requires a very thin quartz plate and the process of thinning down the plate is both time consuming as well as costly and therefore limits the practical max-

imum frequency to a few tens of MHz. The very high lithographic resolution required for SAW IDT at frequencies above 3 GHz increases the effort and cost of fabrication. Furthermore, high losses and limited power handling capability limit the use of high frequencies SAW devices. With increased spectrum crowding, high bandwidth requirements, miniaturization, and low cost requirements, the so called thin film bulk acoustic wave filter technology has been recently developed and is on the way to replace conventional SAW RF-filters in mobile communication applications above 3 GHz as they have now evolved in both cost and performance.

1.2 The thin film electroacoustic technology

Research in thin film electroacoustics has been going on for over 40 years in one form or another [4]. A starting point was the synthesis of high quality zinc oxide (ZnO) films on silicon by reactive sputter deposition, which allowed the development of low cost alternatives to the expensive single crystal SAW devices. Equally so, cadmium sulfide (CdS) thin films grown by vapor deposition were used in combination with quartz as an alternative to BAW quartz resonators for transducers, frequency stabilization and acoustic wave filtering above 100 MHz [5, 6]. Thin aluminum nitride (AlN) films were also studied due to their higher acoustic wave velocity, lower electrical leakage and relatively low temperature coefficient. Difficulties to grow high quality AlN were initially encountered due to insufficient control of impurities during the deposition (essentially oxygen and water), which necessitated the use of ultra-high vacuum systems. Advances in deposition techniques however, such as Physical Vapor Deposition (PVD) systems, allowed highly textured piezoelectric AlN to be grown on a variety substrate materials at low temperatures (<500°C) using reactive magnetron sputtering [7, 8].

The most common materials for thin film EA devices today include AlN, ZnO and lead zirconium titanate (PZT). Extensive research and development of AlN thin film synthesis for high frequency SAW and BAW applications has resulted in that AlN so far appears to be the best compromise between performance and manufacturability and is the prime candidate for mass production of thin film bulk acoustic resonators (FBARs) and filters [3]. Another big advantage of AlN as compared to ZnO is that it is compatible with IC fabrication, both in terms of material and process compatibility. Although the potential of thin film EA devices was demonstrated much earlier [9, 10], it was not until 2001 the first mass produced product entered the RF market, which was a FBAR based 1900 MHz antenna duplexer (transmit-and-receive filter) for mobile phones [11, 12], (see Fig. 1.1.).

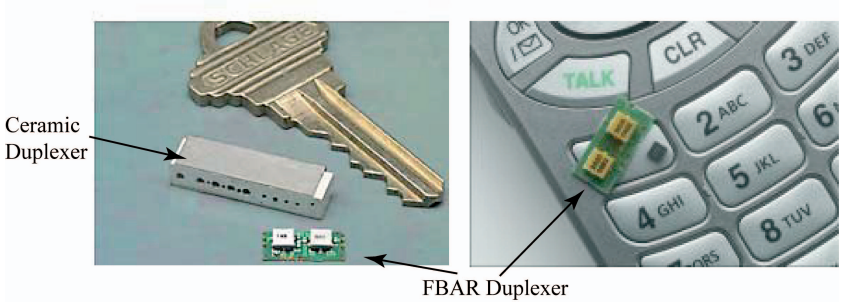

Figure 1.1. FBAR duplexer (2002) from Agilent Technologies.

Today's filter standards put stringent requirements on filter characteristics such as low insertion loss, steep roll-off, large bandwidth, temperature stability, and capability of handling powers up to 1 W, which in turn require resonators with high coupling coefficients and quality factors, in addition to low cost. Although, virtually all commercially available thin film devices so far utilize the BAW or SAW modes there are a number of other wave types and consequently thin film EA devices which exhibit equally competitive performance. These include high velocity lateral propagating waves and their corresponding Lamb wave devices [13].

In conclusion, the thin piezoelectric technology has been recently developed primarily to extend the electroacoustic technology to microwave frequencies [14]. Thin film BAW resonators and filters operating at frequencies ranging from 600 MHz to 12 GHz for military and commercial wireless systems are today a reality [2]. State of the art devices are characterized with small size, good power handling capabilities, low loss and that they can be fabricated on a variety of substrates using essentially the planar technology, which enables mass fabrication of devices at a low cost. As mentioned above this process compatibility and in the case of AlN material compatibility with IC fabrication opens the way for monolithic integration of the traditionally incompatible IC and EA technologies [15, 16], bringing about substantial economic and performance benefits and enabling in addition the further miniaturization of products and components with ever increasing functionality.

1.3 Electroacoustic sensors

In parallel with the development of the EA technology for signal processing applications a variety of EA sensors have also been developed. As a matter of fact, virtually all acoustic wave devices are sensors in that wave propagation characteristics are highly sensitive functions to minute perturbations along the propagation path and/or at its boundaries and hence can be designed to exhibit extreme sensitivities towards small variations in the sur-

rounding medium. Changes of the characteristics of the acoustic wave propagation path result in changes in the wave velocity and/or amplitude hence result in a change of the output signal, i.e. a frequency/phase shift or wave attenuation. Thus, the EA sensor technology includes a wide range of physical, chemical and biochemical sensor applications such as automotive applications (acceleration, torque and pressure sensors), medical applications (biosensors), and commercial and industrial applications (vapor, humidity, chemical, temperature, and mass sensors) [17].

In 1959, Sauerbrey was the first to show that the reduction in resonance frequency (Δf) when an ideal thin film is deposited on the resonator surface is proportional to the change in mass per unit area($\Delta m/A$) [18]. The method of using acoustic waves for mass sensing is based on the gravimetric principle, where the most commonly used mass sensor is the Quartz Crystal Microbalance (QCM) or thickness-shear mode (TSM) resonator, which was initially employed for thickness measurements of thin rigid films in vacuum or in gaseous environments. The QCM is robust, highly sensitive and readily fabricated for frequencies ranging from 5-30 MHz. Advantageous features of QCM are its excellent temperature stability (e.g. AT-cut) and the capability of operating and hence detection in liquid environments, which is essential for biosensor applications. The SAW sensors exhibit an outstanding sensitivity for surface mass accumulation as a result of the confinement of the acoustic energy near the surface region. A serious drawback is that SAWs are poorly suited for in-liquid measurements due to severe acoustic losses into the liquid. There exists a wide range of different sensor types and wave propagation modes, all with varying degree of sensitivity, advantages and disadvantages as well as specific areas of application. The vast majority of these sensors however, are based on single crystalline substrates, which means that the same limitations, as for the signal processing devices, also apply to the sensor field. In this sense, they all suffer from not sufficiently high mass sensitivity for a number of applications resulting from the relatively low frequency of operation since the mass sensitivity according to Sauerbrey is proportional to the square of the operating frequency.

A logical approach to overcome these limitations is to adopt and accordingly adapt the already developed microwave FBAR technology to sensor applications. Regarding gravimetric sensors, a frequency of operation in the GHz range means orders of magnitude higher mass sensitivity. However, the sensor performance is ultimately defined by its mass resolution, which is given by the ratio between the resonator frequency stability (noise level) and the sensitivity. The QCM is very stable with a noise level better than 1 Hz for a QCM operating at 5-10 MHz. The same value for FBARs operating in the GHz range is usually much higher, which results in a mass resolution not significantly higher than that of the QCM sensor [19]. The main benefit using the FBAR technology is therefore not necessarily a very significant improvement in performance but rather to take advantage of the thin film tech-

nology for mass production of low cost and small size sensors. In this way a large number of sensor arrays, monolithically integrated with the associated electronics and other components on a single chip, can be realized.

Physical and chemical sensor transducers based on thin film bulk resonators (FBAR) or solidly mounted resonators (SMR) have shown promising results for mass sensing in air or gas [20, 21]. Attempts have also been made to operate such resonators in contact with liquids for biochemical sensing [22]. However, the longitudinal mode exhibits a significant acoustic leakage into the liquid resulting in a substantial degradation in the Q value and is therefore not suited for biosensors.

The studies performed in this thesis demonstrate unequivocally that AlN based FBARs represent a viable technology for the fabrication of high performance chemical and biochemical sensors. One of the major achievements in this context is the development of a tilted c-axis AlN deposition process, which enables the fabrication of high performance FBARs utilizing the shear mode. Such devices are shown to retain a high Q factor even in contact with a liquid, thus rendering them highly attractive for in-liquid sensing and high resolution biosensors. In parallel with this work there have been a similar development of shear mode solidly mounted resonators (SMR) based on ZnO thin films. Biosensor studies in an avidin/anti-avidin biochemistry have shown an enhanced performance in terms of mass resolution as compared to that of a QCM system under similar conditions [23].

1.4 Thesis outline

The work presented in this thesis includes as follows.

1. Modeling and design of various FBAR structures.
2. Thin film process optimization and material characterization.
3. Device design and fabrication.
4. Electroacoustic measurements and characterization.
5. Extraction and evaluation of device parameters.

The course of the experimental work of the thesis can be divided into three parts summarized in chapters 3 to 5 respectively, where the main objectives are:

- characterize AlN thin film synthesis in order to gain knowledge about the underlying factors determining the performance of EA resonators and to optimize the AlN deposition process for effective shear mode operation(Chapter 3).
- to evaluate and optimize the FBAR design with respect to coupling coefficient, Q value, improved temperature stability, spurious mode

suppression, etc. Develop and evaluate Lamb wave resonators (Chapter 4).

- evaluate FBARs as a viable technology for high resolution mass/viscosity sensors in contact with liquids (Chapter 5).

Chapter 6 gives a summary of the main results, comments and directions for future work.

2 Acoustic Waves and Devices

The purpose of his chapter is to give the reader a brief introduction to the electroacoustic wave theory. To limit the extent of this chapter focus is put on parts related to the devices treated in this thesis and presented in a relatively non-mathematical style. For a more comprehensive exposition of the fundamentals acoustic wave theory the reader is referred to the literature [24].

2.1 Basic acoustic wave theory

Acoustic waves in solids, also known as elastic waves, involve mechanical deformations *strain (S)* of a material and the associated internal forces, which are known as *stresses (T)* [2]. The deformation of a solid composed of atoms or molecules can be represented by *displacements* of the particles from their unperturbed steady state positions. A plane wave generates displacements that vary harmonically in the direction of wave propagation. Further, in the linear plane wave theory the following assumptions are made. For small deformations, the relation between the stress and strain in a body is linear, which in one dimension is known as the Hooke's law, $T = c\,S$ (where c is the stiffness constant). Second, the contours of constant displacements for a plane wave in isotropic solids are *planes* perpendicular to the propagation direction.

In anisotropic solids, i.e. crystals, the propagation of acoustic waves is generally strongly dependent on the propagation direction. The unbounded acoustic wave propagation in an infinite solid described by the *Christoffel* equation [24] results in three general solutions, i.e. three mutually orthogonal plane waves – one quasi-longitudinal and two quasi-shear – each associated with its acoustic phase velocity and particle displacement vector (polarization). The quasi-longitudinal wave exhibits the highest phase velocity and is polarized mainly in the direction of the propagation direction whereas the two slower quasi-shear (transverse) waves are polarized mainly perpendicularly to the propagation direction. The term "quasi" is used to indicate that the polarization vector (parallel or normal) deviates slightly from that in the isotropic case. However, certain crystallographic directions or symmetries yield polarizations that are exactly parallel or perpendicular to the wave propagation and are therefore denoted as pure waves.

The complete representation of stresses and strains in solids requires tensor notation. The elastic stiffness of a solid is fully described by a four rank tensor with a maximum of 81 elements. However, due to symmetry properties of the tensor, a reduced notation can be used resulting in a 6 by 6 matrix, which for the most general solid consists of 21 independent elements. The number of constants reflects the degree of crystal symmetry, as the symmetry increases the number of independent constants decreases. For isotropic solids, e.g. fused quartz (SiO_2), there exists only two independent constants representing one pure longitudinal and one pure shear mode[1]. The phase velocities are independent of the propagation direction and given by

$$v_{long,\,shear} = \sqrt{\frac{c_{long,\,shear}}{\rho}} \tag{2.1}$$

where ρ is the mass density of the solid and c_{long} and c_{shear} are the longitudinal and shear stiffness constants respectively.

Wave propagation in unbounded media can always be represented by these three mutually independent non-dispersive plane waves. Electroacoustic devices, however, are inherently associated with boundaries and wave reflections, which can in general, breed other types of modes that are composed of coupled plane waves where the propagation is strongly dependent of the waveguide and are in some cases dispersive, i.e. the wave velocity is frequency dependent.

2.2 Excitation and detection of acoustic waves

2.2.1 Piezoelectricity

The most common method to generate and detect acoustic waves involves utilization of the piezoelectric effect, which couples mechanical stress to electric displacement (direct piezoelectric effect) and conversely generation of a strain when an electric field is applied to a piezoelectric crystal (converse effect) [25].

Many materials, particularly crystals, exhibit this phenomenon. A necessary property for such a crystal is the non-existence of a center of symmetry. For an unstrained crystal the arrangement of ions (charges) is in such a way that the net charge dipole is zero. Upon mechanical deformation, ions of opposite signs are displaced relative to each other, producing a non-zero dipole and thus an electrical polarization in the crystal; see Fig. 2.1. The

[1] The two shear waves are identical in isotropic media and are therefore degenerate.

converse effect implies a redistribution of the ions (deformation of the crystal), forming dipoles opposite to an applied electrical field. The former effect is used for electrical detection of acoustic waves while the latter is employed for electrical generation of acoustic waves.

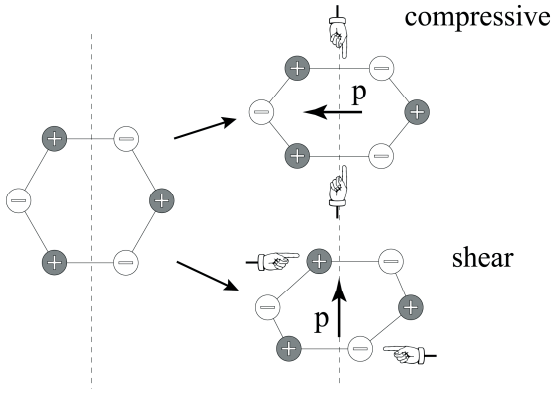

Figure 2.1. Schematic illustration of the piezoelectric effect. Dipole formations are induced by compressive or shear stress.

The coupling between mechanical deformation and electric fields is completely described by the piezoelectric stress tensor or using reduced notation, a 3 by 6 matrix, hence in the most general case, a maximum of 18 piezoelectric stress constants are needed to characterize a piezoelectric material. From crystal symmetry considerations, this number is reduced as the symmetry increases.

However, a specific crystal may be strongly piezoelectric for a given propagation direction while the effect is completely absent in another direction. Hence, piezoelectricity is always "coupled" to the direction of propagation or "cut" of the crystal. Due to the piezoelectric effect, the velocity of propagation of acoustic waves in piezoelectric media is higher than in the non-piezoelectric case. The stiffness constants in that case are referred to as "stiffened" and appear to be larger than their unstiffened counterparts in the non-piezoelectric case. The relative increase of the stiffness constant for a given propagation direction is dependent on the piezoelectric stress, stiffness and dielectric constants associated to that direction according to

$$K^2 = \frac{e^2}{c^E \varepsilon^S}, \tag{2.2}$$

where the superscripts (*E*) and (*S*) in the stiffness constant and dielectric constant denote that they have been measured at constant electric field and constant strain, respectively. The constant K^2 is called the *piezoelectric coupling constant* and is related to the *electromechanical coupling coefficient,*

$$k_t^2 = \frac{K^2}{1+K^2} \tag{2.3}$$

In the literature the former formalism is typically used for laterally excited waves (LTE), whereas the latter is used for thickness excited (TE) waves. It is noted that $k_t^2 \approx K^2$ for $K^2 << 1$ [24].

2.2.2 Transducers and acoustic wave types

A structure that converts an electric-field energy into a mechanical wave energy and vise versa is called an electroacoustic transducer and is in its simplest form a piezoelectric plate or thin film, sandwiched between two metal electrodes. An applied voltage to the electrodes will generate an electric field parallel to the thickness direction of the piezoelectric plate resulting in a deformation of the crystal according to the converse piezoelectric effect. When the transducer is firmly bonded to a propagation medium and excited by a alternating potential – mechanical vibrations in the former will generate acoustic waves propagating into the latter. The lowest frequency of excitation (f_0) is determined by the thickness (d) and wave velocity (υ) of the transducer, $f_0 = \upsilon/2d$. Another very frequently used type of transducer is the interdigital transducer (IDT) originally developed by White et al. [26], which consists of a comb-like metal structure (strip lines) defined on the surface of a piezoelectric material. Application of an alternating voltage between the alternately connected electrodes generates a periodic electric field in the near surface region, which generates a mechanical deformation propagating along the surface. The wavelength (λ) is determined by the distance between a pair of strip lines of equal polarity which also defines the operating frequency (f_0) according to: $f_0 = \upsilon/\lambda$, where υ is the wave velocity. A practical example to illustrate the operation of both transducer types is the two port delay line; see Fig. 2.2. Transducer 1 (transmitter) converts an electrical input signal into an acoustic wave pulse propagating through the wave guide and detected by transducer 2 (receiver), which finally ideally reproduces the electrical input signal. The length (L) of the cavity and the acoustic wave velocity define the time delay (Δt).

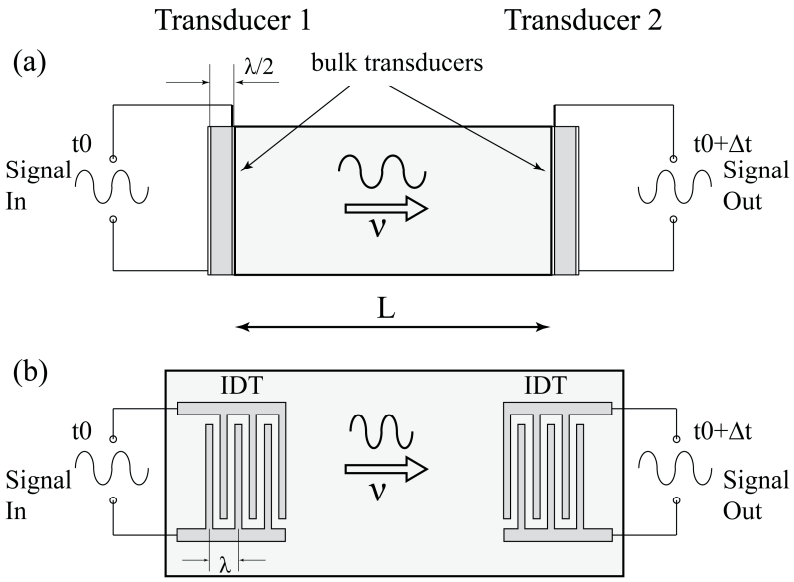

Figure 2.2. Electroacoustic delay line based on; (a) bulk acoustic waves and (b) surface acoustic waves.

These examples of acoustic wave propagation also illustrate the frequently used distinction between bulk acoustic waves (*BAW*) and surface acoustic waves (*SAW*) also known as Rayleigh waves. The former wave type propagates in the bulk of the solid and can be either longitudinally or shear polarized. Typical phase velocities are in the range of 4000-12000 m/s for BAW and 2000-6000 m/s for SAW. The latter wave type propagates at the surface of the wave guide where 90% of the acoustic energy is confined within one wavelength of the surface [2] and is characterized by a combination of longitudinal and shear particle motion. In addition to the above mentioned wave types, a number of other acoustic waves are supported depending on the boundary conditions and the material properties of the waveguide. One such type of wave closely related to SAW is the *Lamb wave* or plate wave which propagates laterally in plates of thickness comparable or smaller than the acoustic wavelength. This wave is divided into symmetric and asymmetric modes to indicate the symmetry of the particle displacements associated with the wave, relative to the median plane of the plate. Generally the plate supports a number of these waves depending on the plate thickness to wavelength ratio. However, for sufficiently thin plates only the lowest order symmetric wave (S_0) and antisymmetric wave (A_0) exist.

The wave types treated in this thesis are restricted to longitudinal and shear mode BAW and symmetric Lamb waves that are experimentally realized as resonator structures. From the fabrication point of view the film bulk acoustic resonator (FBAR) and Lamb resonator devices are similar since

both types require a thin piezoelectric membrane. The way of excitation is generally different even though there are some analogies.

2.3 On some properties of aluminum nitride (AlN)

This section reports on some general properties of thin film AlN.
Typical material parameters and constants that can be found in literature are listed in Table 1. The elements of the stiffness, piezoelectric and dielectric tensors are listed in Table 2.

Table 1. AlN material properties

Parameter	Symbol	Value	Reference
Coupling coefficient (%)	k_t^2	6.5	[27]
Velocity (longitudinal/shear) (x10^3 m/s)	υ_l/ υ_s	11000/ 5800	[28]
Temperature Coefficient (longitudinal) (ppm/°C)	TCF	-25	[27]
Band gap (eV)	E_g	6.2	[29]
Thermal conductivity (W/cmK)	λ	2.0	[29]

Table 2. AlN material constants.

Parameter	Symbol	Value	Reference
Elastic constants (x10^{11} N/m^2)	C_{11}	3.45	[28]
	C_{12}	1.25	[28]
	C_{13}	1.20	[28]
	C_{33}	3.95	[28]
	C_{44}	1.18	[28]
	C_{66}	1.10	[28]
Piezoelectric constants (C/m^2)	e_{15}	– 0.48	[28]
	e_{31}	– 0.58	[28]
	e_{33}	1.55	[28]
Dielectric constants (x10^{-11} F/m)	ε_{11}	8.0	[28]
	ε_{33}	9.5	[28]
Mass density (x10^3 kg/m^3)	ρ	3.26	[28]

3 AlN Thin Film Synthesis

This chapter describes process details regarding deposition of piezoelectric AlN thin films. This is followed by results and a discussion on texture evolution and the underlying determining factors of this process. An original two-stage deposition process for the synthesis of AlN films exhibiting a non-zero mean c-axis tilt is presented. The chapter includes partly results from Papers III – V.

3.1 Reactive sputtering

The vast majority of thin film electroacoustic wave devices are fabricated using reactive sputtering for the deposition of the piezoelectric film. Reactive sputter deposition of compound thin films, namely sputtering of pure metal targets in a reactive gas atmosphere, is a powerful and relatively inexpensive process characterized with a high deposition rate, good control of the film texture and stoichiometry, very good thickness uniformity and surface smoothness, etc. Not the least, sputter deposition is a planar process, i.e. it is part of the IC fabrication. A great advantage of the method is that high quality films can be prepared at near room temperatures on a variety of different substrates including metals with a low melting temperature. Devices composed of multilayer structures where the layers exhibit different thermal expansion coefficients often suffer from intrinsic residual stresses, which can be reduced using low temperature processes. In addition, being a low temperature process makes it extremely promising for integrating the traditionally incompatible EA and IC technologies, particularly in view of back end integration.

All AlN thin film synthesis in this thesis is exclusively performed using *pulsed DC magnetron reactive sputtering deposition*. In view of this a short description of the sputtering process is given as follows (important sputtering process parameters are written in *italic* style):

Sputtering deposition involves transport of material from the target surface in the form of atoms (or clusters of atoms) to a substrate surface where they condense and form a solid thin film. The process is physical in the sense that the atoms in the target are mechanically ejected by means of bombardment with heavy energetic ions generated from a partially ionized gas, i.e. plasma.

Mandatory to all thin film deposition system is the necessity to reduce the incorporation of significant concentrations of impurities into the growing film (e.g. O, C, H_2O for AlN deposition), which in turn requires high performance vacuum systems in addition to high purity target materials (99.999% Al) and process gases (argon, N_2). After evacuation to a *base pressure* below 5 10^{-8} Torr, a controlled constant flow of argon, is introduced into the chamber. The gas flow out of the chamber is subsequently adjusted using a throttle valve thus increasing the pressure to the required process level (i.e. *process pressure*). The plasma discharge is initiated and sustained by means of an electric field where the target serve as the cathode (negative potential) while the grounded chamber walls act as the anode. The substrate located below the target at a fixed distance, *D*, can either be *grounded, floating or biased* (negative potential relative to the plasma), where the latter enables a way to control and enhance the bombardment of the growing film with positive ions of well defined energy.

Reactive, indicates that the sputtered species react with atoms or molecules from the surrounding gas to finally form a compound film on the substrate. Considering AlN sputter deposition, the aluminum atoms are sputtered from the Al metal target while the nitrogen atoms are introduced into the chamber from a gas bottle. Typically a mixture of Ar and N_2 is used since Ar ions cause a higher sputtering rate owing to their larger mass. The *N_2/Ar flow ratio* is an important process parameter for film stress control discussed later.

A **magnetron** represents a target configuration with permanent magnets rigidly attached to the backside of the target configured to generate a strong magnetic field in the vicinity to the target surface and parallel to the latter. As a result of the Lorentz force, energetic electrons traversing the field lines will be trapped and forced to follow spiral trajectories close to the target hence increasing the probability for electron impact ionization. This increases the efficiency of the electron ionization which in turn increases the plasma density and at the same time allows plasmas to be operated at lower process pressures. Consequently, magnetron sputtering is characterized with very high deposition rates, thus decreasing the cost of the process while at the same time reducing the impurity levels in the film. An important parameter in sputter deposition is the mean free path, λ, defined as the average distance a sputtered particle travels before colliding with another particle in the chamber and is inversely proportional to the process pressure. Lowering the pressure will therefore increase λ resulting in an increased λ/D ratio, where *D* is the target to substrate distance. Hence, for values of $\lambda/D > 1$ sputtered particles travel through the gas phase without experiencing multiple collisions and thus retain most of their kinetic energy, which eventually is delivered to the surface of the growing film. In this context, one very useful fea-

ture of the sputtering process and used to its full extent in this thesis is the fact that the sputtered atoms have a relatively high kinetic energy. For instance, the energy distribution of the sputtered particles exhibits a maximum at around half the sublimation energy of the target material. Thus for Al the latter is 3.36 eV which means that the majority of the sputtered Al atoms have an energy of around 1.68 eV, i.e. an effective temperature of 18000^{o}K. Consequently, the condensing atoms have a sufficiently high energy to diffuse along the surface of the film which in turn results in films with very good crystallinity and texture, despite the fact that the actual temperature of the substrate is near room temperature. Note that the temperature of the surrounding gas is also near room temperature and hence if the sputtered atoms collide with it they loose very quickly their kinetic energy resulting in films with poor crystallinity and texture.

Finally, the terms **DC** (direct current), **RF** (radio frequency) and **pulsed DC** refer to the type of electrical power supply employed for powering the discharge. Reactive sputtering of non-conducting compounds, (e.g. AlN, Al_2O_3, SiO_2) results in a partial coverage of the target surface by a thin insulating film of the compound in question. Being non-conductive the surface will eventually charge up if a constant negative potential (pure DC) is applied to the target, thus resulting in problems such as arcing, low sputtering efficiency or in the worst case in extinction of the gas discharge. These problems can be alleviated by applying a short positive pulse to the cathode to discharge the surface of the latter. A pulsed DC power supply is thus characterized by a square waveform where the amplitude and duration of the positive pulse is small relative to the negative counterpart. The amplitude and duration of the positive pulse are generally in the order of a few tens of volts and around ten percent, respectively.

In addition the deposition chamber is equipped with a substrate heater for maintaining *substrate temperatures* up to, say, ~600°C. Figure 3.1 shows an illustration of an AlN reactive sputtering system.

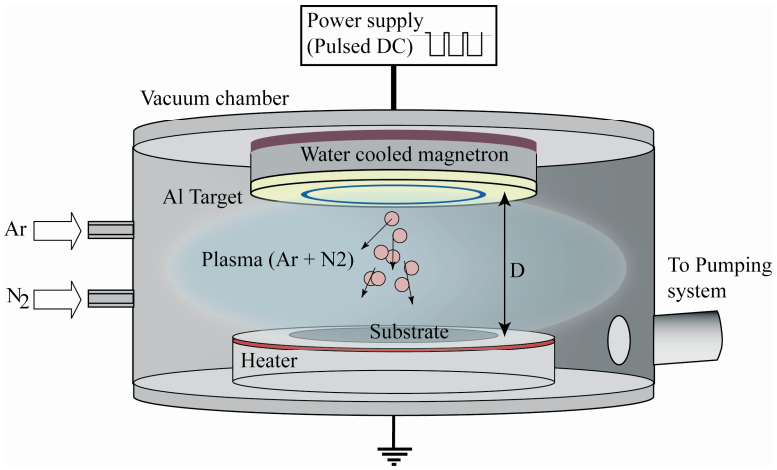

Figure 3.1. Illustration of AlN reactive sputtering deposition system.

3.1.1 Process parameters

The various process parameters in reactive sputtering such as process pressure, plasma density, substrate bias and temperature, gas flow and composition, degree of ion and electron bombardment, etc offer a tremendous flexibility to control and optimize film properties (texture, stoichiometry, stress, etc.) as well as other process related issues (deposition rate, adhesion, etc.). On the other hand this also brings an extreme complexity to the process that requires a deep understanding and optimization of the full set of parameters to achieve a desirable and reproducible result. In addition, the optimized set of parameters is generally system dependent [30], which makes it difficult to directly apply process parameters optimized for other systems. The ground work on optimizing the deposition process of highly textured AlN films used in this work was performed by Engelmark and Iriarte, and is reported in their respective doctoral thesis [31] and [29]. Substantial efforts were devoted to the development of a low temperature synthesis process for SAW and BAW applications, which resulted in the accumulation of significant knowledge about the influence of the various process parameters on film texture [32] and intrinsic stress [33]. It was shown that the process pressure is a determining parameter with respect to the texture of the AlN films grown at near room temperatures. It was argued that the major factor for achieving highly textured growth is the amount of kinetic energy delivered to the growing film by the sputtered atoms themselves (atom assisted growth),

which is most favored at low deposition pressures according to the previous discussion. Under these conditions the film texture was relatively insensitive to other process parameters such as substrate temperature and potential, gas composition and to a certain extent the deposition rate. Based on these results the standard process for c-axis textured AlN used in the work reported in Paper I – III, VI, VII, is given in Table 3. The film stress, which has a tendency to drift with target usage, is controlled by adjusting the Ar/N_2 flow ratio according to [33]. In all cases, no additional heating is provided to the substrate and the maximum substrate temperature due to intrinsic heating is assumed to stay below 100°C.

Table 3. Process parameters

Process Parameter	Value
Discharge power	900 W (pulsed DC)
N_2/Ar flow ratio	varied
N_2+Ar flow	60 sccm
Process Pressure	2×10^{-3} Torr
Base Pressure	$< 5 \times 10^{-8}$ Torr
Substrate Temperature	< 100°C
Substrate bias (Floating)	~ -40 V
Frequency	250 kHz
Duty cycle	13%
Target to substrate distance	55 mm

3.2 Reactive sputtered AlN thin films – growth and microstructure

Considering the electro-acoustic wave technology and devices based on thin films, the correlation between deposition process parameters and film properties is an important issue since the latter affect significantly the device performance.

3.2.1 AlN texture

Piezoelectric AlN belongs to the wurtzite hexagonal crystallographic system and exhibits a 6-fold rotational symmetry around the c-axis (002) plane, which also is the direction that exhibits the highest piezoelectric stress constant in addition to the highest acoustic wave velocity. In electro-acoustic applications one often refers to the c-axis when describing the AlN film orientation. For instance, “oriented AlN film” actually means that the c-axis is parallel to the substrate normal, in the same way the term “inclined films” means that the c-axis is inclined relative to the surface normal. In most cases,

AlN thin films have a polycrystalline, columnar microstructure (see Fig. 3.2) exhibiting some degree of texture or preferred orientation.

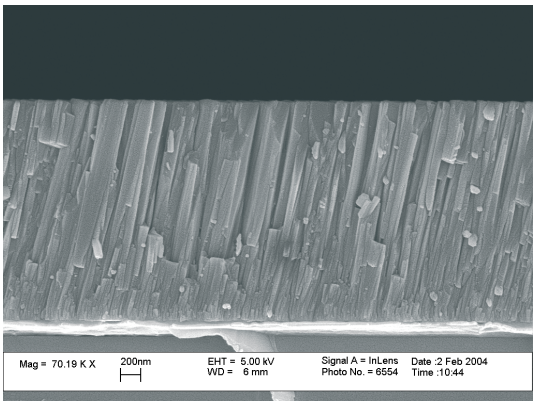

Figure 3.2. Cross section SEM micrograph of an AlN film.

The mechanisms behind texture formation have been studied extensively. These studies indicate that one of the most important processes in this context is the diffusion of adatoms on the surface during the nucleation stage and the diffusion among grains in the growth stage. High diffusion rates generally favor the lowest-surface-energy plane [34], which is the (002) plane for hexagonal AlN. Especially for high temperature processes, AlN shows a strong (002) texture where crystallites can also have an in-plane orientation related to the substrate surface, i.e. epitaxial polycrystalline films [35]. A film with randomly oriented crystallites is referred to as a non-textured polycrystalline film.

3.2.2 Crystallographic characterization

A frequently employed non-destructive method to characterize crystalline materials is X-ray Diffraction (XRD). The film texture (preferred orientation) is readily deduced using XRD θ-2θ scans where the diffraction vector, τ, is parallel to the film surface normal n. The degree of texture for a given crystallographic plane is extracted from the full width at half maximum (FWHM) value of the measured rocking curve peak also known as ω-scan. Accordingly, the diffraction pattern from a highly oriented AlN shows predominately the (002) peak in a θ-2θ (2θ=36°) scan and a minimum FWHM of the (002) rocking curve centered at ω=θ=18°. The scanning range of the ω-scan is limited to the interval $0<\omega<2\theta$ and is therefore not applicable for characterization of AlN films exhibiting a c-axis tilt exceeding 18°. The ψ-scan (psi) is an alternative method to ω-scan that extends the scanning interval to a maximum of $-90< \psi <+90°$. The ψ-scan can be combined with a ϕ-

scan (phi), which yields a two dimensional representation of the c-axis distribution also known as a pole figure. Diffraction in low incidence geometry, i.e. gracing incidence (GI) method enhances the diffracted intensity from the near surface region and is particular useful to characterize films with a low degree of texture since the probed volume is comparatively large. The different XRD measurement geometries employed in this work are illustrated in Fig. 3.3 (a-c).

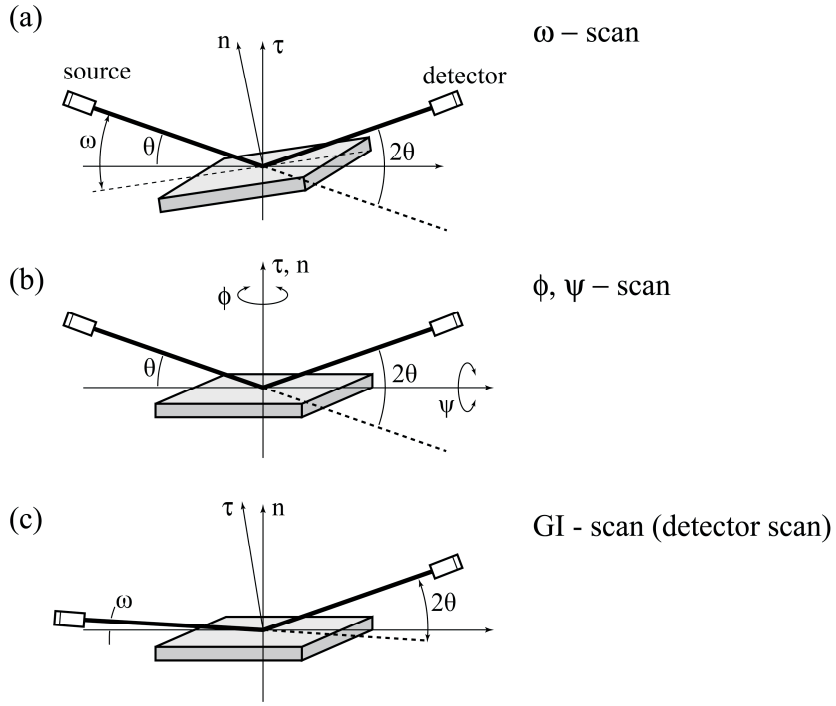

Figure 3.3. XRD geometries. (a) Rocking curve (ω-scan), (b) ψ-scan, ϕ-scan, (c) GI scan (detector scan).

A complete material characterization requires additional methods to analyze its physical and chemical properties. Film microstructure, morphology, surface roughness, etc. can readily be derived from Scanning Electron Microscopy (SEM), Atomic Force Microscopy (AFM) and Transmission Electron Microscopy while Energy Dispersive Spectrometry (EDS), ESCA and Ion Beam Analysis (IBA) methods are employed for analysis of film stoichiometry, chemical state, impurity content, etc.

3.2.3 Influence of the substrate

Thin film BAW, plate wave and in some cases SAW applications involve piezoelectric AlN film growth on a thin metal film. In BAW resonators and

filters where the longitudinal thickness extensional mode is employed, in addition to the process parameters and substrate temperature [36], film texture is also dependent on the substrate surface roughness and crystallographic structure.

The aim of the work in Paper III was primarily to identify which factors and properties of the underlying layer determine the AlN texture. The choice of electrode materials in this study represents materials with different crystallographic structures, surfaces morphology and texture. All AlN films were deposited according to the process parameters given in Table 3 onto aluminum (Al), molybdenum (Mo), titanium (Ti), nickel (Ni), and titanium nitride (TiN) thin films. The AlN film texture was subsequently characterized by measuring the FWHM of the rocking curve of the AlN (002) peak for various degrees of texture and surface roughness of the underlying layer.

The results show an increased degree of orientation of the AlN film for an increasing degree of texture of the underlying films. In addition, the AlN texture worsens with increasing surface roughness. Interesting to note is that a smooth substrate surface does not automatically result in highly textured AlN films. This is especially evident in the case of Ni(fcc,111) and TiN(fcc,111), where the AlN shows a poor texture despite the fact that it was grown on very smooth surfaces. In this case the results indicate that the texture and/or the crystallographic structure of the substrate are the determining factor of the AlN texture. On the other hand, for Ti(hcp,002) that exhibits a relatively high degree of texture, the opposite is observed, i.e. the surface smoothness determines the AlN texture (see Figs.1-4, Paper III). These findings illustrate the need of both well-textured and smooth surfaces in order to grow oriented films. Under these conditions a proper lattice matching between the substrate surface plane and the AlN (002) plane can also promote texture formation [37-39], which in our study can explain the slightly lower FWHM value of films deposited on Ti relative to Al substrates. The lattice mismatch of the AlN(002)/Ti(002) interface is only 4.8% compared to 8.0% for AlN(002)/Al(111). Another general observation (although not without exceptions as indicated above) is that surface structure having a hexagonal symmetry favors textured AlN growth. Thus, fcc metals (Al, Pt) should have a (111) texture, while bcc metals (W, Mo) should have a (110) texture in this context.

3.2.4 Material and device characterization

Even though characterization of film texture, microstructure and morphology gives useful information of the film quality and provides an indirect measure of the piezoelectric properties, other methods are needed to ultimately evaluate the electroacoustic properties of the piezolayer. Direct derivation of the piezoelectric film constants involves measurements of the charges induced upon mechanical deformation [40] and/or conversely the

deformations as a result of an applied external electric field (converse effect) [41]. The latter method requires a very sensitive instrument to detect displacements in the order of a few Ångströms [42] and is typically done by interferometric methods [43]. Electroacoustic measurement using a test structure that resembles the application of interest is a direct measure and the most realistic way to characterize the film regarding its performance from a device perspective. In the most cases there is a correlation between indirect and direct measurements as in the case of electromechanical coupling which has been shown to relate to the degree of texture of the piezoelectric film [36, 44]. However this relationship fails if the film exhibits columnar grains with a mixed polarity, i.e. the film contains grains with anti-parallel c-axis direction. Consequently, such a film will show poor piezoelectricity despite the fact that it is well textured [45]. Another issue related to the performance of a real device is the existence of spurious responses that originate from laterally propagating modes that are more or less always present in the resonator response of interest and cause degradation in Q as well as a not well defined resonance. Methods to characterize such modes include (in addition to direct electroacoustic measurements); 2D and 3D FEM analysis [46, 47] and optical scanning interferometry [48, 49]. One approach to suppress spurious effects is to design the electrode geometry in a way that prevents constructive interference of the lateral waves propagating inside the active area of the resonator [50]. This topic is discussed further in chapter 4 and in a study conducted in Paper II.

3.3 C-axis inclined AlN thin films

In recent years the commercial drive to develop large bandwidth filters has resulted so far in that substantial efforts have been dedicated to optimize c-axis oriented film deposition processes and relatively little attention has been directed towards the development of shear mode resonators. The earliest reports on inclined (and in plane c-axis oriented) films date back to the beginning of the 1970s, where Foster [51] also Minakata et al. [52] demonstrated shear mode operation in ZnO. Wang et al. [53] reported a method for the deposition of tilted ZnO and AlN films for shear mode resonators by applying an additional electric field which is thought to promote tilted c-axis film growth during reactive sputter deposition. Thus, this method requires a specific hardware modification of a standard reactive sputter system. Krishnaswamy [54] deposited tilted films by placing the substrate at a distance from the target center or tilting the substrate.

Very recently shear mode excitation in thin piezoelectric films has gained a lot of interest mainly due to its potential for high frequency resonator operation in liquids and such films are therefore very attractive for the fabrication of highly sensitive biochemical sensors. In a short period of time the

development of shear mode thin film resonators has reached a level of performance comparable to or better than the established QCM sensor technology [19, 23].

The coupling coefficients of both the longitudinal and the shear mode are dependent on the angle between the c-axis and the applied electric field, which angle in the case of thickness excited resonators is equal to the c-axis tilt (θ) relative to the surface normal. Figure 3.4 shows the calculated coupling of the two modes as a function of the c-axis tilt using the Nowotny-Benes (NB) method [55] and material parameters given in Table 2. It is clearly seen that shear mode excitation requires a nonzero c-axis tilt and that the maximum coupling for this mode approaches 5% at 50 degrees. The coupling of the longitudinal mode shows a continuous decrease as the tilt increases.

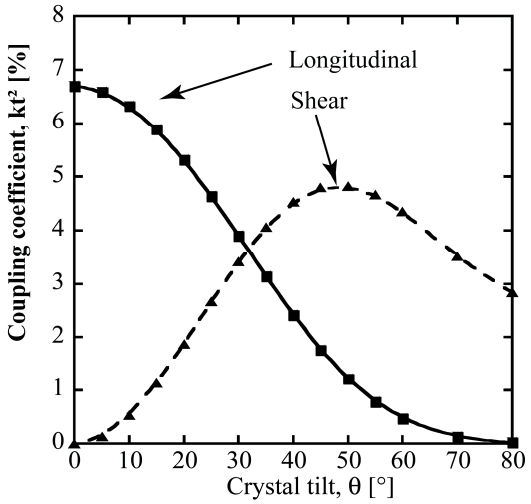

Figure 3.4. The calculated electromechanical coupling coefficient for both shear and longitudinal modes at different AlN crystal tilt, θ, using the NB model.

The synthesis of inclined c-axis AlN is quite challenging particularly in view of the requirements for good thickness and functional uniformity, high coupling and Q, etc. Virtually all tilted film processes presented in literature so far utilize some degree of oblique incidence of the sputtered flux relative to the substrate surface. A trivial way to accomplish this is to tilt the substrate or place the substrate off axis relative to the target. However, films deposited in this way generally suffer from poor thickness uniformity. Another approach is to use a blind placed between the target and substrate in a way that only obliquely incident flux parallel to the blind's blades reaches the substrate. The latter process is characterized with excellent thickness uniformity but suffers from a low deposition rate since only a small portion of the flux reaches the substrate. For high quality AlN films, the deposition rate is criti-

cal since the incorporation of impurities such as O_2 are detrimental to its electroacoustic properties [56]. Thus, an oblique flux incidence is shown to be a necessary condition for inclined c-axis film growth but in general is not the only requirement, as demonstrated in Paper IV. This work lay the ground for the patented two stage deposition process reported in Paper V and has been routinely used for deposition of tilted AlN films for shear mode FBAR and is presented briefly below.

3.4 Tilted film growth – a two stage deposition process

This section summarizes the content in Paper V and presents some additional illustrative measurements regarding characterization and description of the method.

The process is implemented in a standard sputtering system (Von Ardenne-CS 730) as described in section 3.1 without any hardware modification. The substrate is typically positioned parallel to and centered directly under the target. In its typical implementation the process consists of two stages. In stage 1, a special layer, here in referred to as the seed or nucleation layer, is grown at high a process pressure (20 mTorr) to a thickness around 100 nm. The other parameters are set according to Table 3. This seed layer is fundamental to the process as it is characterized with a large population of (103) nano-crystallites with a random in-plane orientation of the c-axis. This is achieved as the process is operated at a relatively high pressure, under which conditions the relatively energetic Al atoms sputtered from the target experience multiple collisions in the gas phase, resulting in their thermalisation before condensing onto the substrate surface. Noting that the substrate is at near room temperature, the film growth is said to be in a diffusion limited regime resulting in a significant nucleation of (103) oriented grains. This sets the stage for phase 2 of the process which is done at a pressure of 2 mTorr, under which conditions the condensing Al atoms experience negligible energy losses in gas phase collisions, so that growth proceeds in the so called competitive growth regime. In other words, the growth now proceeds along the fastest growing planes, which are the c-planes of the (103) grains facing the mean flux direction at the point under consideration. As the latter has a circular symmetry it is clear that the mean c-axis tilt of the film will also exhibit a circular symmetry over the wafer.

3.4.1 Tilted Film analysis

The mean c-axis tilt (directed towards the center) for films synthesized according to this scheme ranges from 25 to 30 degrees over the wafer excluding a minor circular area in the center where the mean tilt approaches zero; (see ψ-scans in Fig. 4, Paper V). A clarification regarding the mean tilt con-

cept might be in place here. Consider the ψ -scan taken at the near center region of the wafer (see Fig.4, Paper V). The intensity distribution is nearly symmetric with two local maxima at ± 26º. The interpretation of this observation is that in this area there exist grains tilted equally amount but with opposite direction, and therefore cancel each others' piezoelectric contribution. The pole figures in Fig. 3.5 (a) provide a 2D representation of the c-axis distribution at the same point where the circular distribution further illustrates the symmetry in the center of the wafer. Figure 3.5(b) represents a measurement taken 35 mm from the center of the wafer and clearly shows a highly non-symmetric distribution with a mean tilt of around 28º. The intensity distribution along the ψ –axis represents the c-axis tilt distribution in the *r-n* plane, where *r* is the vector in parallel with the wafer radius and *n* is the surface normal, and is analogous to the 1D distribution in Fig. 4, Paper V. The elliptical shape of the 2D contours represents the c-axis tilt distribution out of the *r-n* plane and is a consequence of the circular tilt symmetry.

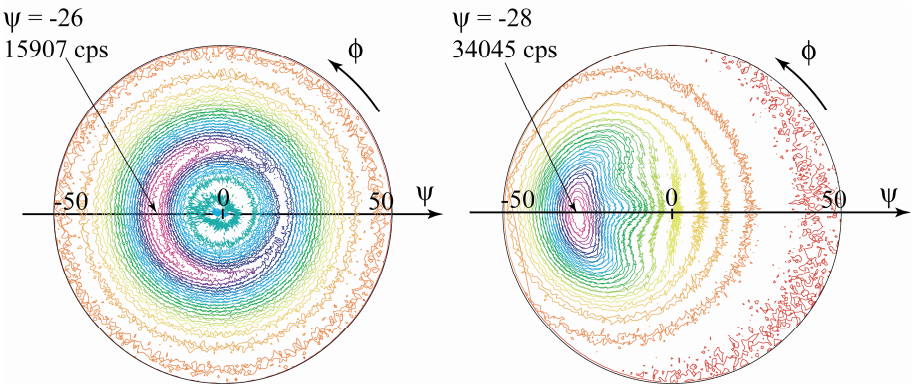

Figure 3.5. Pole figures taken (a) close to the center and (b) 35 mm off center.

In order to fully characterize the film a series of electroacoustic measurements were performed on resonators located along the radius of the wafer. Figure 3.6 shows the coupling coefficient and Q value as a function of the distance from the center.

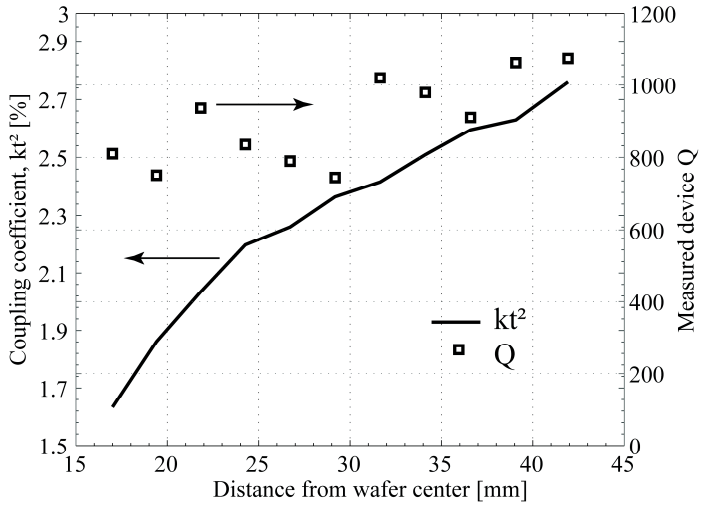

Figure 3.6. Electromechanical coupling and Q value as a function of the distance from center of the wafer.

3.4.2 Discussion

Generally, there are two conditions that need to be satisfied in order to achieve tilted film growth;

- ✓ Favorable surface structure and/or morphology for tilted grain nucleation.
- ✓ Oblique incidence of the net deposition flux.

With respect to the first of these two conditions the seed layer has to have a poor (002) texture (preferably have a (103) texture) and/or have a relatively high surface roughness. This is accomplished by using a high process pressure which is known to result in poorly textured films. Figure 3.7 shows GI scan diffractograms of two equally thick (100nm) seed layers deposited at 20 and 2 mTorr, respectively. The GI geometry here is adjusted to allow Bragg reflection of highly textured AlN films as evidenced by the strong (103) reflection for the 2 mTorr film which indicates a high c-axis texture[2]. The 20 mTorr film has, however, a relatively low degree of texture. In addition, this film exhibits a significantly higher surface roughness (*RMS=1.84 nm*) compared to the 2 mTorr (*RMS=0.39 nm*) film as illustrated by the AFM micrographs in Fig. 3.8. Note the different scales.

[2] For ω=5º, the 2θ angle and diffraction vector (τ) coincide with the (103) inter plane distance and direction, respectively, which for an oriented film is 28º off normal.

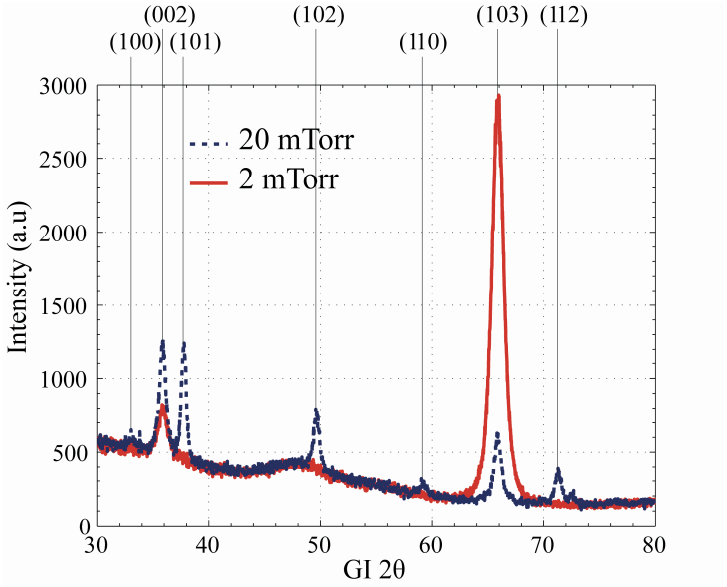

Figure 3.7. XRD GI-scan of two 100 nm thick AlN films deposited at 20 and 2 mTorr, respectively.

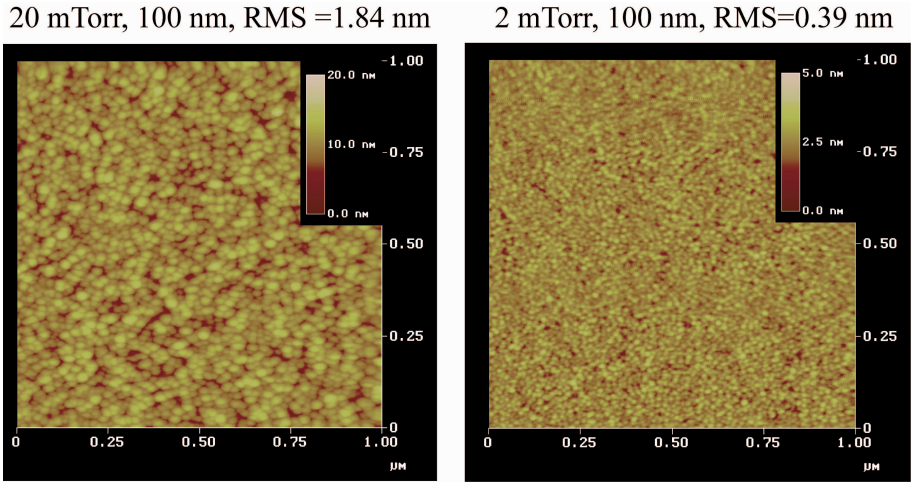

Figure 3.8. AFM micrographs of 100 nm thick AlN deposited at 20 and 2 mTorr, respectively. The surface roughnesses (RMS) are 1.84 nm (20mTorr) and 0.39 nm (2 mTorr), respectively.

Once favorable nucleation conditions are established, tilted growth in stage 2 is achieved through the directionality of the deposition flux at the substrate surface, which for a finite target is asymmetric for all points on the substrate except in the center of the wafer, provided that no significant scattering of the sputtered flux takes place in the gas phase; see illustration in Fig. 3.9.

The latter is guaranteed by the process pressure which is such that the mean free path of the sputtered particles is comparable or larger than the substrate-to-target distance.

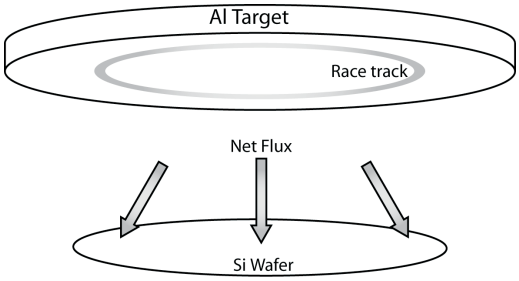

Figure 3.9. Directionality of the net flux from a finite target.

Under these conditions the film growth process proceeds in the so called competitive growth regime, that is, cones receiving largest flux grow fastest as argued above. It is noted that the mean tilt as a function of the wafer radius approaches rather quickly an angle of around 30º and remains constant right up to the edge of the wafer, despite the fact that the mean flux direction varies considerably along the wafer radius. This observation supports strongly the hypothesis made above that it is the (103) oriented grains in the seed layer that give rise to the tilted growth since the c-axis of a (103) oriented grain makes an angle of 28º with the surface normal. Thus it is concluded that the crystallographic texture of the substrate (seed layer) is of utmost importance for a tilted growth. The second necessary condition is the non-normal incidence of the mean deposition flux at the point under consideration.

Alternatively, in cases where the substrate surface possesses significant roughness, tilted film growth is also possible even without necessitating a particular crystallographic texture of the substrate (as discussed in Paper V). In such cases, stage 1 is omitted and nucleation is dominated by (002) grains parallel to the substrate surface. Since the latter is rough, then the c-axis of the grains relative to the mean surface normal exhibits a broad distribution. Hence, growth proceeds along the cones whose c-planes are oriented towards the incident flux. Evidently, in this case the mean tilt will exhibit a monotonous increase along the radius of the wafer.

4 Thin Film AlN Resonators

The devices studied experimentally in this thesis are AlN thin film resonators of membrane type including FBAR and Lamb wave devices. This chapter gives an overview of the FBAR technology with emphasis on basic resonator parameters such as coupling coefficient, Q value, spurious modes, temperature stability, etc. In this work the FBAR is specifically employed as a test structure for electroacoustic characterization of AlN film and evaluation of both longitudinal and shear wave propagation in the thickness direction. Simulation and modeling of FBARs and parameter extraction are discussed with emphasis on the modified Butterworth-VanDyke (MBVD) lumped-parameter circuit and the one-dimensional Nowotny-Benes model. Further, temperature compensation is required in a number of critical applications. This chapter includes a method based on an intrinsic temperature compensation of FBARs utilizing a SiO_2/AlN composite structure. An optimized design combining temperature compensation, retained frequency of operation, coupling and Q value using the second harmonic shear mode propagation has been achieved, which demonstrates that temperature stable high resolution FBAR sensors for in in-liquid operation can be realized.

At the end of this chapter, resonators based on Lamb waves are addressed and different approaches of excitation are discussed.

4.1 Film bulk acoustic wave resonators

Generally, a BAW resonator is a transducer where the generated electro-acoustic waves stays confined within the resonator cavity by means of acoustic wave reflections at the resonator surfaces, as a result of which the internal electroacoustic wave pattern consists of both incident and reflected waves. It is the interference of these waves that causes the resonance conditions (standing waves) that dramatically alter the electrical characteristics of the resonator.

Consider the thickness excited (TE) BAW resonator in Fig. 4.1. The resonator volume is defined by the thickness (d) and the overlapping area between the top and bottom electrodes (also called active area), here repre-

sented by a square[3] with a side length L. Depending on the orientation of the AlN film, longitudinal and/or shear waves are excited and propagate in the thickness direction. The resonance frequency is determined by the thickness of the piezolayer together with the thickness of electrodes and the acoustic wave velocity in each respective layer. For infinitely thin electrodes however, the resonance condition is established for, $N\lambda = 2d$, where λ is the wavelength and N is an integer. The antiresonance frequencies are then given by [24]

$$f_a = \frac{v_a}{2d} N \tag{4.1}$$

where v_a is the wave velocity. Even though this structure acoustically supports all harmonics, only odd harmonics are electrically excited (an asymmetrically applied field only couples to an asymmetric displacement distribution), hence $N = 1, 3, 5, etc.$ The displacement distribution of the fundamental mode ($N = 1$) is illustrated in Fig. 4.2. The displacement is zero in the film center and reaches its maximum at the surfaces of the resonator.

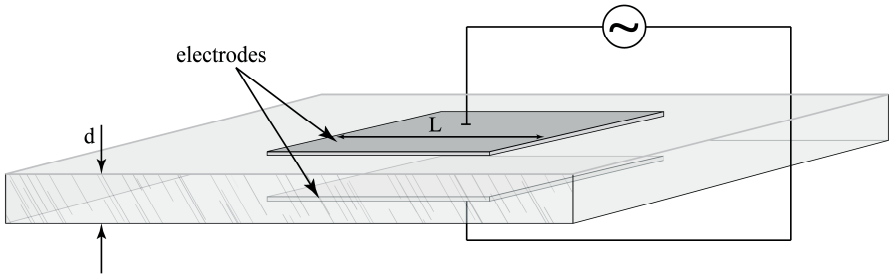

Figure 4.1. Schematic of a thickness excited BAW

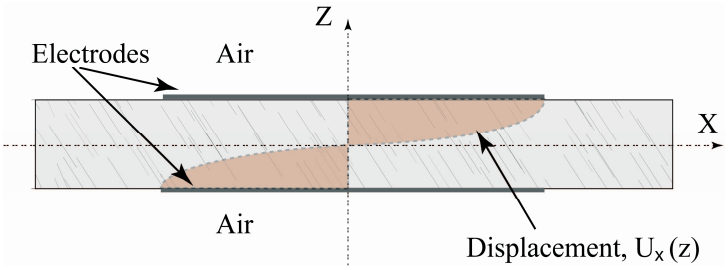

Figure 4.2. Displacement distribution of the thickness propagating fundamental mode ($N=1$)

[3] Electrode geometry has no fundamental significance for the excitation of acoustic waves in the thickness direction, but is directly related to lateral wave propagation.

The characteristic electrical input impedance for an ideal resonator without losses is shown in Fig. 4.3(a) for a frequency sweep including the fundamental and third mode. At frequencies outside resonance, the impedance response is dominated by the static capacitance (originating from the metal-dielectric-metal structure), thus the impedance magnitude is proportional to *1/f*. A closer look at the near resonance region discloses a dramatic change of both the impedance magnitude and the phase; see Fig. 4.3(b). Two characteristic frequencies can be distinguished; the frequency at zero impedance (infinite admittance) and the frequency at infinite impedance (zero admittance). These frequencies are denoted as resonance (f_r) and antiresonance (f_a) respectively, and define the lower and the upper boundary of the inductive region (*i.e. phase = +90*) for any given harmonic.

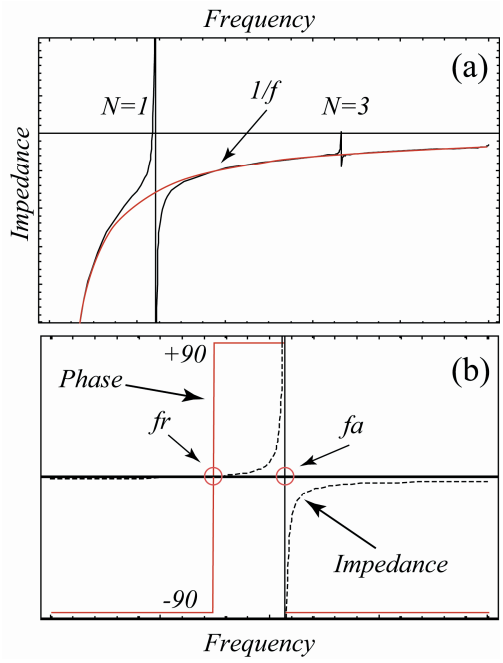

Figure 4.3. (a) Wide band impedance versus frequency response (b) narrow band phase and impedance response, definition of the resonance f_r and antiresonance f_a frequencies.

4.1.1 Resonator quality factor (Q)

The resonator quality is one of the most important parameters in EA applications. In FBAR based filters, high Q resonators are of vital importance for achieving low insertion losses as well as a steep roll-off, i.e. rapid change from the band-pass region to the out-of-band rejection region

[11]. Low phase noise oscillators and high resolution sensors require resonators with a high Q and high short term frequency stability.

There exist a number of loss mechanisms (both electrical and acoustic) that result in a reduced Q value. Resistive losses in the electrodes and dielectric losses in the piezoelectric layer are examples of electrical losses. Non-ideal electrical isolation of the electrodes and contact pads from the substrate results in parasitic losses and degraded performance too. Acoustic losses in materials can be attributed to a range of factors. First, an intrinsic loss due to internal friction is inherent to all materials, which limits the maximum material Q value. The *intrinsic Q* is inversely proportional to frequency such that the $Q \cdot f$ product is constant and is often used as a figure-of-merit (FOM) when comparing resonators operating at different frequencies [57]. Material defects such impurities and grain boundaries are sources of acoustic losses and are particularly Q-degrading if the they are close to high stress areas, i.e. close to a nodal plane of the resonator [57, 58]. Wave scattering losses due to roughness at interfaces and surfaces is also detrimental to the resonator quality [59, 60]. Improvement of resonator quality requires optimization of the film deposition processes to reduce material defects particularly in layers subjected to significant strain levels. Further, the electrode material and geometry are important factors determining the overall Q. The geometry in particular can be of significant importance in suppression of unwanted (spurious) modes that contribute to the acoustic energy dissipation [61]. Techniques to suppress such modes are available as discussed in section 4.4. A prerequisite for high Q operation is to minimize the acoustic energy radiation into the surroundings. This is effectively accomplished in membrane type FBAR where the adjacent medium is air or gas.

The existence of losses in the resonator results in a non-zero impedance at resonance and consequently a finite value of the real part of the admittance (i.e. conductance). The frequency at maximum conductance defines the series resonance frequency (f_s) and in the same manner, the parallel resonance frequency (f_p) is defined as the frequency at maximum resistance [62]. The quality factor is generally expressed as the ratio of the energy stored and energy dissipated during one oscillation cycle [24]. A practical method to derive the *device Q* directly from the resonator impedance is

$$Q = \frac{f}{2}\left|\frac{d\phi_z}{df}\right|, \tag{4.2}$$

evaluated at either the series or parallel resonance frequency and were ϕ_z is the impedance phase [63]. Alternatively, one can derive Q from the -3 dB bandwidth of the admittance response at series resonance [64].

4.1.2 Electromechanical coupling coefficient (k_t^2)

For sufficiently high Q values as well as for small fractional difference between the resonance and antiresonance frequencies the resonator electromechanical coupling coefficient is approximately given by [24]

$$k_t^2 = \frac{\pi^2}{4}\frac{f_p - f_s}{f_p}. \tag{4.3}$$

The frequency separation of (f_s) and (f_p) depends on both the piezoelectric material coupling factor and the electrode material as well as electrode thickness. This is demonstrated by Lakin et al. [27], where an optimized electrode configuration resulted in an enhanced effective coupling exceeding the bulk piezoelectric material coupling. Thus an electro-mechanical coupling of 7.7% was achieved for AlN FBAR at 1880 MHz using a combination of aluminum and tungsten electrodes (the bulk value along the c-axis of AlN is 6.5%). As the thicknesses of the electrodes are increased further the effective coupling decreases, which is a consequence of the relative increase of piezoelectrically "dead" material in the resonator cavity. The possibility to tune the effective coupling in this way provides an additional degree of freedom in filter design. Nevertheless, accurate derivation of the resonator parameters is important in filter design where the properties of individual resonators determine the overall filter performance [63]. Therefore, a quantity describing the resonator performance in terms of effective coupling coefficient and the resonator figure of merit (M) has been used particularly in the filter literature [62]

$$k_{eff}^2 = \frac{f_p^2 - f_s^2}{f_p^2} \tag{4.4}$$

$$M = \frac{k_{eff}^2 \cdot Q}{(1 - k_{eff}^2)} \tag{4.5}$$

The relative difference of the two definitions (4.3) and (4.4) is ~10% for $f_s/f_p < 0.97$ ($k^2_{eff} < 6\%$). The rather big discrepancy requires that care must be taken when comparing coupling coefficient values in the literature. However, in this work measurements of the coupling are often associated with comparative studies, where qualitative behavior rather than exact values is of primary interest.

4.1.3 Electroacoustic characterization and modeling

The electroacoustic characterization of the resonators in this work is typically done with one port measurements of the reflection coefficient (S_{11}) using a Hewlett Packard 8720D (Hewlett-Packard, Palo Alto, CA) network analyzer (NWA). All devices were wafer probed using a picoprobe calibrated for a 50-ohm system. Equivalent circuit representation is useful for evaluation of the resonator performance and extraction of material properties from measurements. Once the lumped parameters of the resonator are known circuits of greater complexity can be studied in circuit analysis programs. The modified Butterworth-VanDyke (MBVD) lumped-parameter circuit illustrated in Fig. 4.4 is representative for one-port resonators with negligibly thin electrodes [64]. Under certain conditions, i.e. when the electrodes can be regarded as a mass loading, this model also holds for resonators with thick electrodes [65]. The accuracy of the MBVD model is restricted to a narrow range of frequencies near the resonance frequency and valid only if the mode in question is sufficiently isolated from other modes. The physical parallel plate capacitor formed by the electroded dielectric structure is represented by three elements; the capacitance (C_0), dielectric loss (R_0) and electrode resistance (R_s), respectively. The acoustic wave contribution is represented by a L_1-C_1-R_1 circuit parallel to C_0, often referred to as the "motional arm" and is related to the electroacoustic properties of the materials used. L_1 and C_1 are the motional inductance and capacitance, respectively, while R_1 is the motional resistance representing the acoustic attenuation. The series resonance (f_s) is set by L_1-C_1 reactance cancellation resulting in a real valued input impedance defined by (R_s + R_1), while the parallel resonance (f_p) is defined by C_0 in parallel with L_1 and C_1.

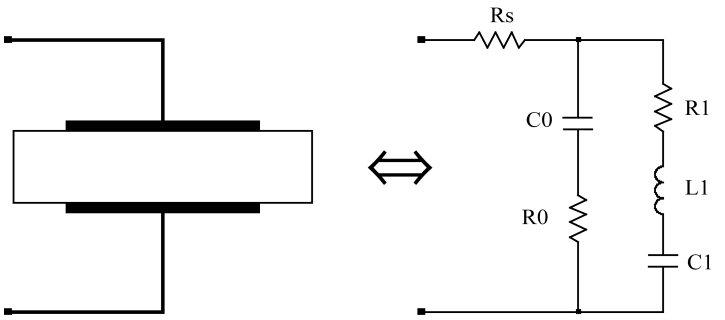

Figure 4.4. MBVD equivalent circuit representation of a thickness excited resonator.

f_s, f_p and the *extracted intrinsic Q* value at series resonance (i.e. the electrode electrical loss excluded) are given by

$$f_s = \frac{1}{2\pi}\frac{1}{\sqrt{L_1 C_1}} \tag{4.6}$$

$$f_p = \frac{1}{2\pi}\sqrt{\frac{C_0 + C_1}{L_1 C_0 C_1}} \tag{4.7}$$

$$Q_s = \frac{\sqrt{L_1 / C_1}}{R_1} \tag{4.8}$$

It is noted that the above model is only representative for resonators where the major loss mechanisms can be described by the three resistive elements. Depending on the design of electrodes, contact pads and choice of substrate material, etc., there can exist significant external parasitic contributions (inductances, capacitances and resistances) that must be accounted for in the model. The work with identifying those parasitics can be quite challenging and care should therefore be taken already in the design stage. Nevertheless, provided that the model sufficiently represents the measured device – a good fit between measured and calculated response can be achieved using a least mean square optimization procedure. This kind of optimization tools is available as commercial computer software, e.g. Advanced Design System (Agilent Technologies Corp.). Methods based on an iterative procedure for parameter extraction are however rather time consuming (several minutes) and therefore not practical when characterizing a large number of devices. Full scale wafer mapping of several thousands devices per wafer requires fast extraction and an automated data acquisition system in order to be feasible [64].
Paper I describes an alternative fast direct extraction technique of the elements in Figure 4.4 based on the same principle as reported in [66].

It is understood that the extraction procedure can be omitted if the use of lumped parameters is of secondary importance hence the device Q or coupling can be directly derived from the measured data using (4.2, 4.3).

4.1.4 Resonator modeling and simulation

While the MBVD model is convenient for parameter extraction and evaluation a more physical approach is needed to predict the complete frequency response of a resonator structure. Accurate modeling of piezoelectric resonators requires a full three dimensional (3-D) model which involves, in general, the application of numerical methods such finite element simulations [47]. Both 3-D and 2-D FEM [46] are helpful in the lateral design of FBARs and can give valuable information about

undesirable lateral propagating modes (spurious modes) and their dependence on resonator topology. These methods, however, are rather computer resource intensive. In many cases – especially in the initial stages of device development – a simpler one-dimensional treatment is sufficient to predict a resonator response, e.g. resonance frequencies, effective coupling, etc. Provided that the physical geometry is close to 1-D accurate results can be achieved despite that complex structures involving stacks of many layers are analyzed. Two popular 1-D models are the Mason model [24], based on a transmission line representation of the resonator stack, and the Nowotny-Benes (NB) model [55] where each layer is described by an 8x8 transfer matrix. Both methods use an analytical approach to calculate the frequency response based on the material parameters (density, stiffness, piezoelectric and dielectric tensors) of each layer and geometrical dimensions (thickness and area).

The analysis of both the TE longitudinal and shear mode requires a simulation tool that allows analysis of resonator response for an arbitrary tilt of the crystal. This is readily achieved with the NB model by applying a straightforward rotational transformation of the AlN material parameter tensors. The model was expanded to also account for the temperature dependence of the materials involved for the characterization of an Al/AlN/Al/SiO_2 composite resonator, see section 4.3.1 and Paper IX. The calculated temperature coefficients of frequency (TCF) for the first and second harmonic longitudinal and shear mode showed a remarkably good agreement with the measurements. Resonance frequencies and coupling coefficients of the various modes are readily calculated but the resonator Q value is infinite as long as the material losses are neglected. The full potential of the model is illustrated in Paper VIII, where resonator operation in contact with viscous media is demonstrated both theoretically and experimentally.

4.2 FBAR fabrication

Thin film BAW resonator fabrication employs micro-machining techniques in combination with deposition methods for depositing the thin piezoelectric film and metal electrodes in a sandwich-like structure either as an edge supported freestanding membrane or solidly mounted to an acoustically isolated substrate. The former is referred to as a film bulk acoustic resonator (FBAR) and the latter solidly mounted resonator (SMR). The FBAR is the most straightforward structure to fabricate and requires ideally, deposition of a minimum of three layers (electrode – piezoelectric film – electrode) onto the carrier substrate. A typical thickness of the piezoelectric film is a few microns while that of the metal electrodes is an order of magnitude less. To acoustically isolate the resonance cavity, parts of the substrate are removed to create a freestanding membrane or alternatively a sacrificial layer is used

to create an air (gas) cavity beneath the resonator. The high acoustic impedance mismatch in the solid/air interface results in an effective reflection of the acoustic waves and a minimum acoustic radiation to the surroundings hence enables high Q resonance. The SMR isolation to the substrate is ensured by an acoustic mirror (Bragg reflector), which consists of a multilayer of $\lambda/4$ thick alternating high and low acoustic impedance materials. Both types have their advantages and disadvantages but the fundamental difference is that SMR structure has a superior mechanical robustness in addition to not being equally prone to spurious effects. The SMR approach allows fabrication on various substrates as long as the substrate surface is smooth enough which is readily achieved by using standard chemical-mechanical polishing (CMP). The latter makes the SMR technology particularly viable for large scale integration with active devices. The freedom to choose low cost substrate materials (e.g glass) is advantageous from an economic perspective. The SMR is also able to accommodate larger intrinsic film stresses, which in the FBAR case can result in severe problems with membrane buckling or cracks. On the other hand, manufacturing a mirror requires several additional layers, each with a well defined thickness (especially at high frequencies) and low surface roughness, resulting in a higher degree of process complexity and higher fabrication cost. The SMR approach has the potential of increasing substantially the power handling capabilities [67] of the thin film EA technology and make it attractive for base station applications.

The fabricated BAW resonators in this thesis are solely of membrane based FBAR type mainly because of their simplicity and the potential to achieve high Q and coupling coefficient. Another advantage is that both surfaces are accessible which is particularly useful in FBAR sensor applications since the liquid or gas can be supplied to the bottom side (bottom electrode) thus providing easy access to the topside for on-wafer electrical probing. Further, the risk of parasitic electrical losses when measuring in liquids is minimized since the bottom electrode is normally grounded[4]. The FBAR fabrication process is described in greater detail in Papers IV, V, IX. Typical resonators are composed of 200 nm thick bottom and top aluminum electrodes and 2 μm thick AlN film deposited on a high resistive, 100 cm in diameter silicon wafer substrate using a DC planar magnetron sputtering system Von Ardenne-CS 730. Standard lithography and dry/wet etching processes are employed for film patterning. The resonator membrane is acoustically isolated from the supporting Si substrate by etching the latter from the backside of the wafer using a highly anisotropic three-step dry etch Bosch process. The thickness excited (TE) resonator thus fabricated is used for electro-acoustic characterization of AlN films or for evaluation of FBAR

[4] The bottom electrode is normally in physical contact with the substrate which is generally grounded.

operation in liquid media. The latter requires a microfluidic transport system for delivering the liquid to the bottom electrode surface and can be done in the same step as the release of the membrane by using the aspect ratio dependence on the etch rate. Figure 4.5 shows a SEM micrograph illustrating the aspect ratio dependence for Si dry etching using the Bosch process. By designing the channel width smaller than the membrane area – release of the latter can be achieved, leaving enough silicon in the smaller channels to ensure mechanical robustness of the channel structure. The channel is completed by sealing the etched cavity channel structure from the backside, see Fig. 4.6.

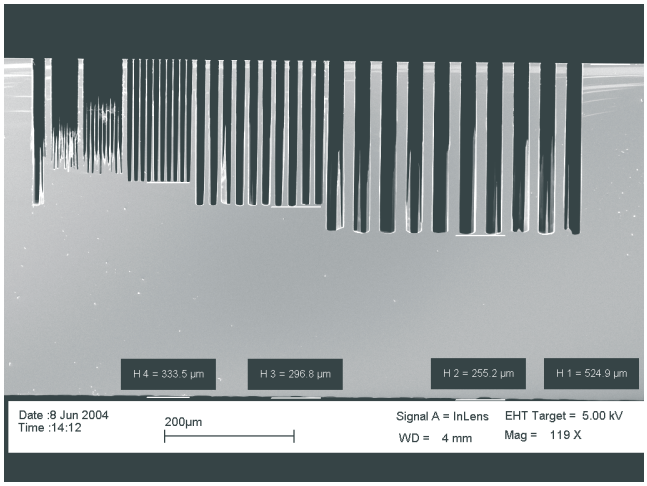

Figure 4.5. Aspect ratio dependency for the Bosch silicon etch process.

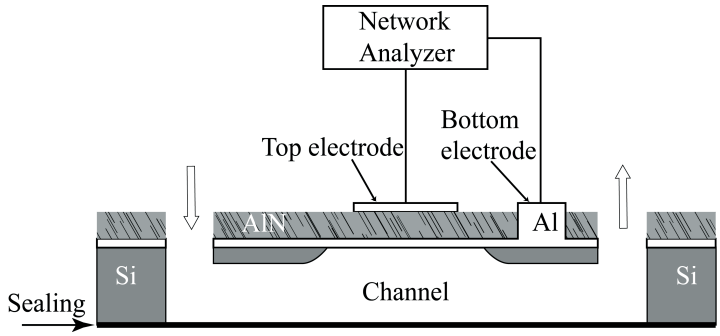

Figure 4.6. Illustration of FBAR with microfluidic channels defined in the bulk substrate.

4.3 Thermal stability

A critical issue in EA applications is the temperature stability of the FBAR's. Non-compensated filters for instance, must be designed to have a larger than required bandwidth to accommodate band edge shifts due to temperature variations. Temperature stable resonators are mandatory in highly stable oscillator applications. Further, thermal fluctuations in electroacoustic sensors increase the signal noise and instability which in turn decreases the sensor resolution.

All materials have (to a varying degree) temperature dependent material constants (stiffness, expansion, dielectric, etc) which results in a change in the acoustic wave velocity and device dimensions. Accordingly this will entail a change in resonance frequency. Temperature stable piezoelectric materials are only available in single crystalline form and then for special crystal cuts only. The well known AT cut in quartz exhibits an excellent thermal stability around room temperature [25]. An effective but rather impractical technique to avoid frequency shifts due to temperature variations is to stabilize the temperature of the environment using an oven. Alternatively, a thermo-element in the vicinity of the resonator can be used to measure the temperature and subsequently derive a temperature independent resonance frequency, provided that the f vs T dependence is known for the temperature interval of interest. Another standard approach is the so called differential method which requires some kind of a reference point, say, two separate resonators (oscillators) where one serves as a reference. A similar technique without using a reference resonator is reported in [68]. This dual band approach utilizes both the fundamental and third mode to separate the frequency shift due to difference in mass loading and the temperature change effect in QCM.

The thin film technology offers an additional way to achieve temperature compensation, as described in the following section.

4.3.1 Temperature compensation

In comparison with AT-QCM, both AlN and ZnO are rather sensitive to temperature variations. The relative frequency shift or the temperature coefficient of frequency (TCF) is expressed as;

$$TCF = \frac{1}{f_0}\frac{\Delta f}{\Delta T}10^6 \quad [\text{ppm/ºC}] \tag{4.9}$$

where (f_0) is the resonance frequency. The majority of piezoelectric and electrode materials exhibit a negative TCF value, i.e. the frequency decreases with temperature. For an AlN based FBAR this value is typically around -25

ppm/ºC for the longitudinal mode and even higher for ZnO (-60 ppm/ºC) [27]. Compensation of this negative TCF can be achieved by incorporating into the resonator cavity an additional layer of a material that exhibits a positive TCF. A suitable material for this purpose is silicon dioxide (SiO_2, +85 ppm/ºC) [69], which can be thermally grown SiO_2 or deposited using reactive sputtering for instance. This method has been employed for temperature stabilization of both SAW [70, 71] and BAW [53, 69, 72] devices. A drawback of this method is the reduced effective coupling as a result of the incorporation of a piezoelectrically "dead" material in the resonator volume. In filter applications this results in a reduced effective bandwidth. Figure 4.7 shows a cross-section SEM micrograph of a composite FBAR structure composed of 2μm AlN, 200nm top and bottom Al electrodes and a 1.2μm thick thermally grown SiO_2. This composite structure exhibits an effective TCF close to zero (in a limited temperature range) if the thickness ratio of positive and negative TCF materials is properly chosen. Equally interestingly, this configuration also allows the excitation of even harmonics and in particular the second harmonic which has been studied in greater detail in this thesis. Specifically, it is demonstrated that the thickness ratio can be tuned in such a way (see Fig. 4.9) as to obtain both good temperature compensation as well as a high coupling coefficient, not much lower than that of the non-compensated first harmonic. The final result is that we have two devices (one non-compensated and operated at the first harmonic, and one compensated and operated at the second harmonic) such that both operate at practically similar frequencies, both have similar coupling coefficients, both have similar Q values, the only difference being that the second one is thermally stable as discussed in greater detail below.

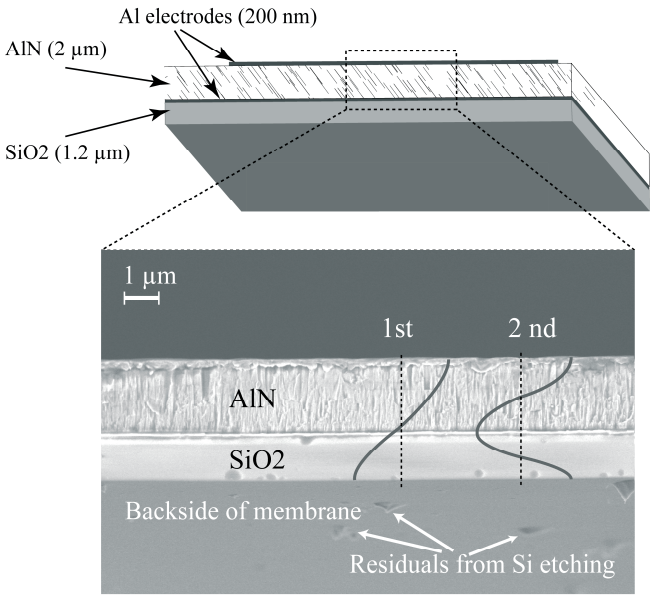

Figure 4.7. Illustration and cross section SEM micrograph of a Al/AlN/Al/SiO_2 composite membrane.

Figure 4.8 shows the TCF of a composite AlN/SiO_2 resonator for the first and second harmonic shear modes calculated at room temperature for the following two different cases: A) The temperature dependence of the electrodes is neglected and B) when the temperature dependence of the electrodes is included in the simulations. It is noted that in the calculations a 25^o tilt of the c-axis is assumed since this is the mean c-axis tilt of the films grown according to the process described in chapter 3. Evidently, the temperature behavior of the four-layer stack is strongly dependent on the temperature coefficients of the electrode material. This is easily understood in terms of the strain energy density distribution. Most generally, the increase of the oxide thickness is expected to provide increasing temperature compensation. However, when considering a multi-layer system, the distribution of the strain energy density in the different layers should also be taken into account [73]. Thus, the initial increase of the oxide thickness leads to a significant increase in the strain energy density in the bottom Al electrode, which in turn increases its influence over the device response. The latter effect counteracts the temperature compensating contribution of the oxide itself and leads to an initial degradation of the TCF.

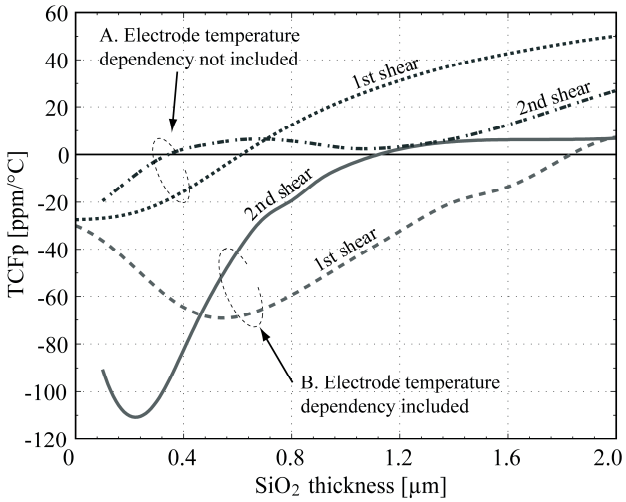

Figure 4.8. Simulated TCF at room temperature for the first and second harmonic of the shear mode versus SiO_2 thickness for two different cases: The temperature dependence of the electrodes has been omitted (curves A) and included (curves B) in the simulations.

Further, the SiO_2 layer loads the resonator and thus reduces its resonance frequency[5], as shown in Fig. 4.9(a). The first harmonic shear mode frequency at a SiO_2 thickness of around 1 μm for instance, has decreased to almost half the non-compensated value at zero oxide thickness, which for this mode is around 1.3 GHz. It is also seen that the coupling coefficient of the same mode is continually decreasing with the thickness of the SiO_2 layer, Fig. 4.9(b). The second harmonic shear mode shows a similar decrease in frequency but has a much higher frequency to begin with and maintains it higher throughout the entire thickness range. In addition, the coupling of the first shear mode decreases monotonically with oxide thickness, while for the second harmonic shear a maximum in coupling is observed at an oxide thickness of around 1.3 μm as seen from Fig. 4.9(b). This is attributed to the fact that the most effective excitation is achieved when the thickness of the AlN film equals one half-wavelength of the standing wave [74], see the insets in Fig. 4.9(b). For the second harmonic mode this condition also means that one-half-wavelength of the standing wave is confined within the compensation layer.

[5] For fixed AlN and electrode thicknesses.

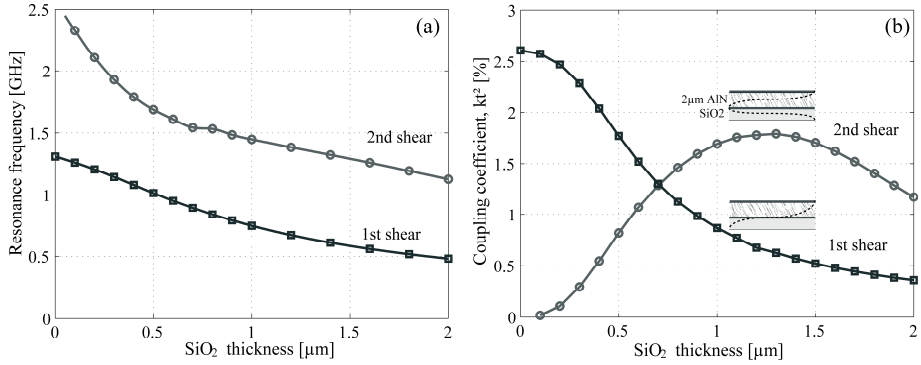

Figure 4.9. (a) Resonance frequency and (b) coupling coefficient as a function of SiO_2 thickness for constant AlN thickness.

As the result is uniquely determined by the materials, layer thicknesses and relative position in the stack, various combinations are possible to achieve compensation for a specific mode. The freedom of design however is highly reduced when other parameters such resonance frequency, coupling coefficient, Q value and process related issues are taken into account. The work in Paper IX demonstrates a resonator optimized for in-liquid operation where the second harmonic shear mode proved to be an optimal choice in view of thermal compensation on the one hand and retaining resonator performance in terms of coupling, operating frequency, Q value, etc on the other. Nevertheless, the above discussion also illustrates the need for accurate modeling when analyzing complex structures and making optimal design.

4.4 Spurious modes

Spurious modes are unintentionally excited modes and are undesired in the sense that they interfere with the mode of interest causing “ripples” in the frequency response. In the case of thickness excited resonators the origin of these spurious modes are generally laterally propagating waves that are coupled to the main thickness excited mode, where the most pronounced one is the first order symmetric Lamb mode (S_1). This mode is partly trapped by the abrupt borders of the active resonator area defined by the electrode periphery and causes higher order standing waves inside the resonator volume at frequencies roughly, $f_n=n(v_l/2L)$, where n is the mode number, v_l the lateral wave velocity, and L the lateral electrode dimension, see Fig. 4.1. Lateral waves that escape from the active resonator volume and propagate out into the supporting substrate contribute to the overall acoustic energy losses and hence degrade the device Q which is particularly a problem for FBARs since the membrane outside the active area, easily supports lateral propagating

waves. A frequently used method to analyze the spurious phenomena is to measure the wave amplitude by optical interferometry and transform the data into dispersion (ω-k) diagrams. The dispersion diagrams indicate which modes are supported by the lateral dimensions of the resonator and can create standing waves at specific frequencies. There exist two main approaches to suppress spurious waves, both involving some kind of modification of the top electrode edge design. The most effective method includes an additional mass loading confined to the edges of the electrode and is referred to as lateral resonator edge design [75]. By adjusting the thickness and width of this layer, spurious modes are effectively suppressed as the additional mass loading creates conditions for destructive interference between the reflected waves. This method is shown to be particularly effective for SMRs [75]. The second method utilizes an irregular top electrode geometry and is known as apodization and has been employed to smoothen out the spurious resonances in the FBAR response [61, 76]. This latter method is further studied in Paper II which explores various electrode geometries to reduce the problem with the lateral modes. Apodization (or irregular electrode geometry) in this case also destroys the condition for constructive interference between the incident and reflected waves and hence results in a substantial reduction of the amplitude of the standing waves inside the resonator active area, providing a smoother resonator response. This can, for instance, be accomplished to a certain extent by employing a non-parallel electrode edge design, see Fig. 4.10. The electrode geometries (a-b) can easily be understood to support lateral standing waves between the borders. In contrast, the electrode geometries in (c-d) prevent constructive interference between the reflected waves inside the borders. It is noted that this method is unable to stop lateral leakage but offers on the other hand a relatively easy way to achieve a smooth response.

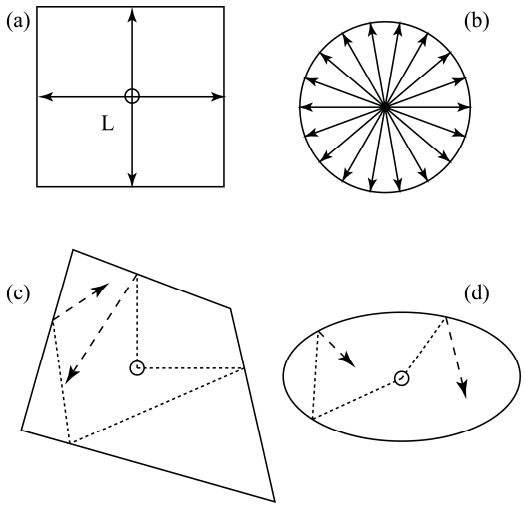

Figure 4.10. Different electrode geometries. (a-b) shapes that create conditions for a constructive interference (c-d) shapes where constructive interference is minimized

4.5 Lamb wave resonators

As noted in the introduction the drive towards high frequency applications has pushed the traditional SAW technology towards its practical limits. For a given substrate material the frequency is determined by the spacing of the interdigital transducer fingers which in turn is limited by the resolution in the optical lithography defining the IDT pattern. An alternative method to increase the frequency is to use high acoustic velocity substrates or a combination of piezoelectric and high velocity materials in layered structures. AlN/diamond structure is an excellent example that is known to support surface wave velocities exceeding 10000 m/s [77, 78]. A further method is to utilize high velocity modes such as the symmetric Lamb mode in thin film membranes. Lamb waves or plate waves propagate laterally in plates of a thickness comparable or smaller than the acoustic wavelength. In contrast to the previous section where lateral waves caused energy loss and degraded the performance of the thickness mode, in this case they themselves are employed for the design and fabrication of high frequency devices. Lamb waves are divided into symmetric and asymmetric modes to indicate the symmetry of the particle displacements relative to the median plane of the plate. Generally the plate supports a number of these waves depending on the plate thickness to wavelength ratio. However, for sufficiently thin plates only the lowest order symmetric wave (S_0) and antisymmetric wave (A_0) exist. The symmetric mode shows the highest phase velocity of the two and is therefore suitable for the fabrication of high frequency devices. The antisymmetric mode can be designed to carry waves with a velocity lower than

the sound velocity in liquids thereby making it suitable for liquid sensor [79]. Both AlN/Diamond layered SAW and AlN membrane Lamb waves are dispersive, i.e. the wave velocity is not solely determined by the material constants but also by the ratio between the thickness of the piezoelectric layer and the wave length defined by the IDT pitch. Figure 4.11 shows the wave velocity as a function of d/λ for the two lowest SAW modes and the S_0 Lamb mode. It is noted that all modes exhibit very high velocities as the normalized AlN thickness is decreased. Further, by the slope of the curves one can deduce the velocity- thickness sensitivity which from the fabrication point of view is important in terms of sensitivity to process variations and hence defines the process window. By designing the device to operate in a plateau region an otherwise very strict thickness control requirement can be relaxed, thus lowering the requirements on the deposition process. In view of the latter, the S_0 mode is most favorable since it has a low dispersion in addition to exhibiting a high velocity for membrane thicknesses below 0.3λ.

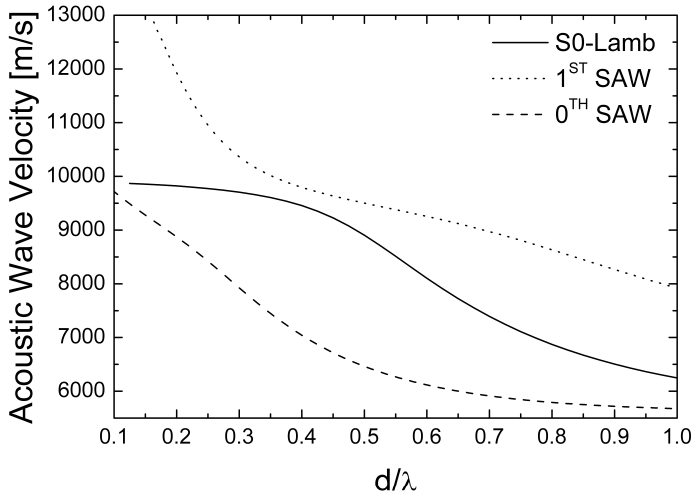

Figure 4.11. Acoustic wave velocity as a function of the AlN relative thickness.

There are two major aspects concerning the design of Lamb devices. The first one is related to the way the wave is excited while the second one concerns the design of the reflectors on the limited area of the AlN membrane. With respect to excitation there are two main approaches that can be used. The first is based on the inter-digital transducers IDT concept [80] while the second one employs longitudinal/lateral field excitation (LFE) [81]. Both make use of grating structures but can be configured differently to apply an electric field in the thickness direction of the plate in order to excite Lamb waves. In Paper VI it was found that the latter is advantageous due to a larger effective coupling to Lamb waves for c-axis oriented AlN. In addition, a

very high wave velocity was observed, $v_{lamb}=10298$ *m/s*, allowing the fabrication of high frequency resonators with *Qxf* products better then $0.5x10^{12}$ s^{-1}. Lamb resonators can be realized by defining $\lambda/4$ reflector gratings on each side of the transducer in the same manner as for SAW resonators. This approach was further analyzed in Paper VII in a comparative experimental study of different topologies including IDT and LW based Lamb wave excitation. A drawback with the LW approach is the somewhat more complex fabrication since the definition of a bottom electrode grating requires an additional process step. Evidently, growing an AlN film on such a structure is not optimal since there is a tendency of formation of micro-cracks in the AlN film in the vicinity of the steps of the underlying grating, see Fig. 4.12.

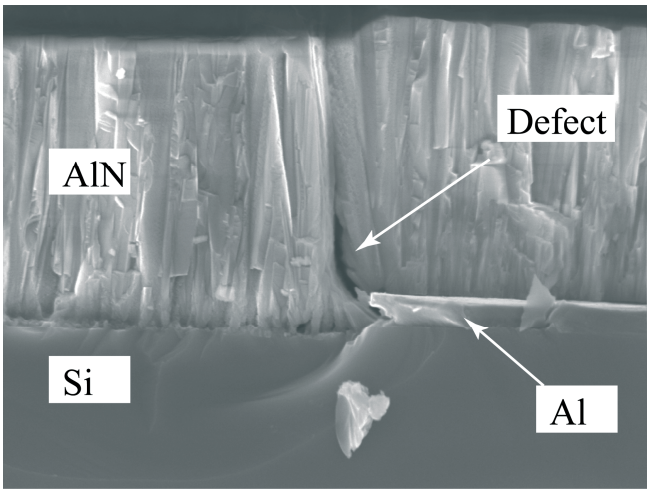

Figure 4.12. Defect in the AlN film initiated by a step in the Al electrode.

This can be avoided by using a continuous bottom electrode thus providing a flat surface for the deposition of high quality AlN films [13] or by using buried electrodes as reported in [82].

Although the initial design was not optimal it is clear that the symmetric zero order Lamb mode in thin AlN membranes, owing to its extremely high velocity, can be used for the fabrication of low cost, IC compatible electroacoustic devices by means of standard resolution photolithography up to the lower gigahertz frequency range. In subsequent studies [13] the design was substantially improved yielding a *Qxf* product close to $3x10^{12}$ s^{-1}.

5 FBAR Sensors

In this chapter we take a look at an emerging sensor technology based on the use of FBARs as sensing elements in sensor applications and in particular such that require resonator operation in contact with liquids. In the course of the work in this thesis, various processing steps, design approaches and experimental setups have been developed for the fabrication and characterization of FBARs as high resolution in-liquid sensors and ultimately as biosensors and chemical sensors. The tilted film deposition process described in section 3.4 has been routinely employed in the experimental work in this thesis to achieve effective shear mode operation and hence high sensitivity and excellent Q values even in contact with liquids.

5.1 QCM vs FBAR

Quartz Crystal Microbalance (QCM) based sensors represent a mature sensor technology, characterized with high resolution and relatively low cost. Today QCM resonators find a variety of applications ranging from physical (mass, pressure, etc) through to chemical and biochemical sensors. If the FBAR technology is to be competitive it has to excel its QCM counterpart in either cost and/or performance. QCM and shear mode FBARs are similar in that they both utilize the thickness excited shear mode, but there end the similarities. The fundamental difference is the frequency of operation. A typical FBAR studied in this work resonates in its fundamental thickness shear mode at around 1 GHz, which means 100 to 200 times higher frequency than a standard QCM operating in the 5-10 MHz range. In theory this means much greater mass sensitivity for the FBAR since the latter is proportional to the square of the operating frequency. This tremendous gain in sensitivity, however, is partly negated by the loss in stability as the losses are linearly proportional to frequency and hence the mass resolution (defined as the ratio between stability and sensitivity) only scales as *1/f*. The gap is further reduced by the inferior temperature stability of FBARs combined with their inferior material Q as they use polycrystalline films. All these factors indicate that a theoretical comparison between the two technologies does not produce a clear cut and detailed experimental studies are needed to develop and demonstrate the advantages of the FBAR sensor technology.

Preliminary resolution studies performed in this thesis indicate that the mass resolution of FBAR sensors is not significantly greater than that of QCM. These are not definitive results, however, as the measurements were done in a network and not in an oscillator mode. Significant efforts are currently being made both in Europe and in the rest of the world to perfect the FBAR sensor technology. Perhaps among its greatest advantages is the small size (3 orders of magnitude smaller than QCM) as well as their low cost stemming from the enormous productivity of the planar fabrication technology. In addition, the small size opens the way for making sensor arrays and powerful bio-analytical tools together with associated electronics on a single chip.

5.2 Mass sensitivity

The most common electroacoustic sensing application is based on the gravimetric principle for mass detection. The presence of displacement maxima on the resonator surfaces makes the resonator resonance frequency very sensitive to surface mass accumulation which can be understood from energy conservation principles. Every conservative mechanical system can be described by an conversion between potential energy (U_p) and kinetic energy (U_k) such that the total energy is conserved at all times. The former term is derived from the deformation (strain) and material stiffness constants where the latter is dependent on the mass density and displacement velocity. A slight perturbation of the surface density (ρ_s) caused by a uniformly distributed mass accumulation (Δm) on the surface area (A) will cause an increase in the kinetic energy while the potential energy remains unaltered. Since the total energy must be constant (from energy conservation) it follows that the wave velocity is accordingly reduced, which in turn results in a reduction of the frequency as [25]

$$\Delta f = -\frac{2f_0^2}{\rho_q \upsilon_q} \cdot \frac{\Delta m}{A} = -\frac{2f_0^2}{(\rho_q c_q)^{1/2}} \cdot \rho_s \tag{5.1}$$

where (f_0), (ρ_s) are the unperturbed resonance frequency and the areal mass density of the accumulated layer, and (ρ_q), (c_q), and (υ_q) are the piezoelectric layer mass density, stiffness constant, and wave velocity, respectively. This expression is only valid when the added mass consists of an ideal thin rigid film attached rigidly onto the surface so that it moves synchronously with the oscillating surface. Further, since this model was originally developed for QCM devices (where the relative electrode thickness is small), it is also assumed that the influence of the electrodes can be neglected. However, for a FBAR this assumption is not justified since a typical resonator operating in the GHz range has a significant fraction of electrode material in the resona-

tor volume and is in this sense a composite structure. In this context, an FBAR represents a heavily loaded resonator where the influence of the electrodes on the sensitivity cannot be neglected. In practice it is necessary to use more accurate theoretical methods and models for determining the mass sensitivity. Thus, using the NB model, realistic FBAR structures are readily modeled for arbitrarily thicknesses of the additional layers and their relative positions in the stack.

By way of example, consider the temperature compensated resonator in section 4.3.1 operating at the second harmonic at around 1.3 GHz. The relative thickness of non-piezoelectric materials in the structure is substantial in addition to being asymmetric in the thickness direction. The calculated frequency shift as a result of mass loading with Al_2O_3 is shown in Fig. 5.1 for two cases; (a) the mass is added onto the SiO_2 surface and (b) the mass is added onto the Al top electrode surface. The relative mass sensitivity defined as

$$S_r = \frac{1}{f_0}\frac{\Delta f}{\Delta \rho_s} \tag{5.3}$$

for case (a) is 960 cm^2/g and is somewhat lower than that in case (b) namely, 1240 cm^2/g.

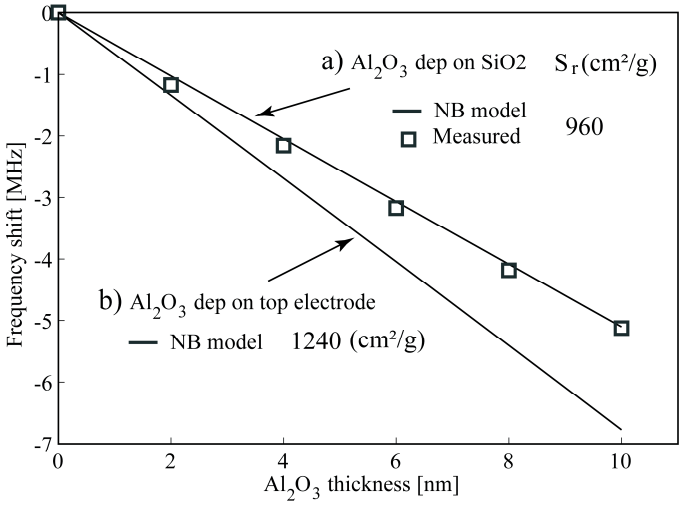

Figure 5.1. Modeled frequency shift for Al_2O_3 deposition on to (a) the SiO_2 surface and (b) the top electrode. (squares) Measurement in case (a).

The experimental measurements (squares) for case (a) show a good agreement with the theoretical predictions. Since the sensitivity is related to the amount of acoustic energy transmitted into deposited layer the acoustic matching between materials becomes relevant. In the above example the lower sensitivity in case (a) is attributed to a lower degree of acoustic energy

in the SiO_2 layer as a consequence of a partial reflection of the wave in the interface between the bottom electrode and the SiO_2 layer.

In conclusions the sensitivity is not only dependent on the operating frequency but also on the materials in the resonator stack, where relative positions of the layers in the stack, thickness and acoustic matching to the material being sensed all play a role.

5.3 Resonator stability

The most important property of a mass sensor is its mass resolution, defined as the smallest detectable surface mass density. As noted earlier this quantity is set by the ratio between the resonator stability and sensitivity. Short-term-frequency-stability is influenced by both internal noise and noise introduced by fluctuations in the environment. However, it is known that the frequency stability is dependent on the resonator Q value and maximizing Q helps reduce the minimum detectable mass density [83]. There exists an IEEE standard procedure suggesting how to calculate the noise of oscillators from data sets in the time domain commonly known as the Allan deviation [84]. This procedure has been the general approach to determine the stability of our resonators and its primary use here has been for qualitative comparison between resonators. It is noted that these measurements were performed under non-controlled conditions, i.e. in an ordinary office environment without taking any precautions regarding temperature drift, humidity, vibrations, dust, etc. A typical noise evaluation includes 100 subsequent measurements (series and/or parallel resonance) with a 10 s time interval. It is noted that this parameter is not optimized with respect to the minimum deviation and the result from stability characterization is therefore assumed to be underestimated in general. Further, additional noise caused by the measurement equipment has not been taken into account. A typical Allan deviation value ranges from $5x10^{-7}$ to $5x10^{-6}$ for a non-compensated resonator. In terms of resolution this corresponds to a value *0.5-5 ng* cm^{-2} for a resonator exhibiting a mass sensitivity equal to *1000* cm^2 g^{-1}.

Operating a resonator in a liquid is always associated with acoustic losses radiated into the liquid, i.e. energy is dissipated which and reduces Q. Several factors are involved and discussed further below. Before that, it is noted that the issue of energy dissipation into the liquid is particularly important for the FBARs under study in this work since the mode normally employed is not pure, i.e. it is quasi-shear. This means that the mode degenerates at the liquid interface into pure shear and longitudinal modes respectively, since liquids exhibiting isotropic elastic properties. Confining the discussion to the longitudinal mode, a fraction of it leaks out into the liquid, resulting in a loss of Q and consequently resolution. Clearly, the most optimal texture is a-axis where the TE mode is pure shear.

5.4 In-liquid resonator performance

Whether an acoustic wave can be used for practical in-liquid sensing depends on the particle displacement relative to the surface normal. Longitudinal BAW and SAW for instance, exhibit displacements perpendicular to the surface and thus generate compressional waves propagating into the liquid, resulting in severe acoustic losses and Q degradation. BAW shear waves are associated with in-plane displacements which couple to the liquid through internal friction forces at the interface and which forces depend on the viscosity of the liquid. Assuming no-slip, the very near surface liquid layer moves synchronously with the resonator surface and couples motion into the liquid. Since liquids do not support shear waves the amplitude of the motion decays rapidly with distance from the surface. The characteristic length or decay length (δ), depends on the angular frequency (ω), liquid viscosity (η) and density (ρ) as given by [25]

$$\delta = \left(\frac{2\eta}{\omega\rho} \right)^{1/2} \tag{5.4}$$

The decay length in water at 5 MHz is 250 nm [25], whereas at 1 GHz this value is one order of magnitude less (~20 nm) , reflecting a fundamental difference between QCM and FBAR operation in liquids.

The coupled liquid layer closest to the surface increases the kinetic energy and causes a decrease in frequency proportional to the square root of the $\eta \cdot \rho$ product according to Kanazawa [85]

$$\Delta f = -f_0^{3/2} \left(\frac{\eta\rho}{\pi\rho_q c_q} \right)^{1/2} . \tag{5.5}$$

However, the shear frictional motion in the near surface region represents energy radiated into the liquid and causes a reduction in Q. The frequency shift can be represented as an increase in motional inductance (L_1) while the acoustic loss due to energy dissipation can be seen as an increase in the motional resistance (R_1), (see Fig. 4.4) in the equivalent circuit. This motional resistance leads to resonance damping and is ideally proportional to $(\eta \cdot \rho)^{1/2}$. It is noted that this model assumes smooth surfaces and laminar flow while the coupling to the liquid is through viscosity only. In reality there can be additional factors that result in deviations from above calculations. Rough surfaces can cause non-laminar flow and also out-of-plane motions that will increase the motional elements [86].

Figure 5.2 shows the response of a shear mode FBAR at 1.28 GHz operated in air and pure water. The Q value as derived from the impedance phase

slope according to (4.2) is around 800 in air and drops to 195 in water. The corresponding shift in frequency is around 2 MHz.

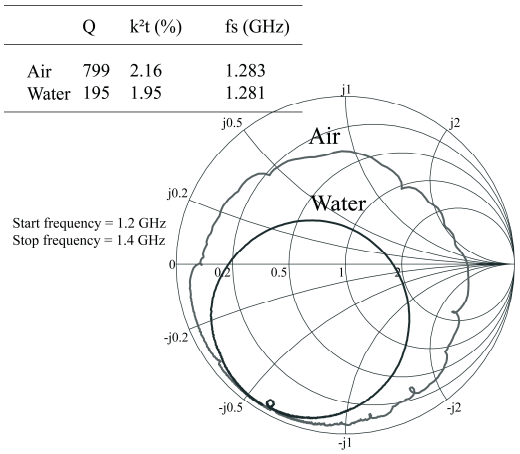

Figure 5.2. Resonator response in air and water plotted on a Smith chart.

The dissipation (*1/Q*) due to viscous load is defined as $D_{visc\_load} = D_{tot} - D_0$, where D_{tot} and D_0 are the total dissipation and dissipation in air, respectively. The dissipation when immersed in water for the above resonator is accordingly *1/195-1/799 =0.4%*. Usually it is difficult to separate the dependence on the viscosity and the density of the liquid. A classical experiment is to utilize the practically insignificant density variation of glycerol as a function of its concentration to study the resonator performance as a function on viscosity only [86]. Paper VIII reports on measurements and simulations of resonator operation in water-glycerol solutions (0-70%) representing an equivalent viscosity ranging from 0.01 to 0.20 P. This paper also addresses the influence of the quasi-shear nature of the wave on the resonator performance in liquids through comparison between measurements and predictions using two different models - the Kanazawa theory discussed above and the NB model respectively.

5.4.1 Mass loading in a liquid

The next issue is how to characterize mass loading effects in liquid environment and which approaches the limits of this thesis. Initial results are reported in [87]. Here, a comparative study between the shear mode FBAR and QCM using a competitive antibody-antigen association process is performed. The study is the first reported in the literature to have successfully demonstrated an FBAR biosensor and is shown to have a similar performance regarding the sensitivity for detection of cocaine and heroin molecules.

5.4.2 Microfluidic system

For accurate and reproducible measurements of high frequency resonators in liquids, stable measurement conditions are required to avoid unwanted interference from the environment. In addition, the analyte or liquid must be delivered to the sensing surface in a controlled way. This is accomplished by a special flow injection system consisting of a peristaltic pump and an injector which allows a stable and reproducible supply of the liquid to the resonator surface.

Figure 5.3 shows a schematic illustration (a) and photograph (b) of the measurement setup for in-liquid characterization. The liquid is fed into the on-chip micro-fluidic system through a miniature steel pipe, which in turn is sealed with an o-ring to the wafer surface. An identical piping is provided at the outlet for draining the liquid. This set up allows continuous on-wafer measurements without having to dice the individual resonators. An indirect method to verify whether the resonator is in contact with the liquid is to monitor the Q value of the longitudinal mode, which drops significantly due to the liquid load.

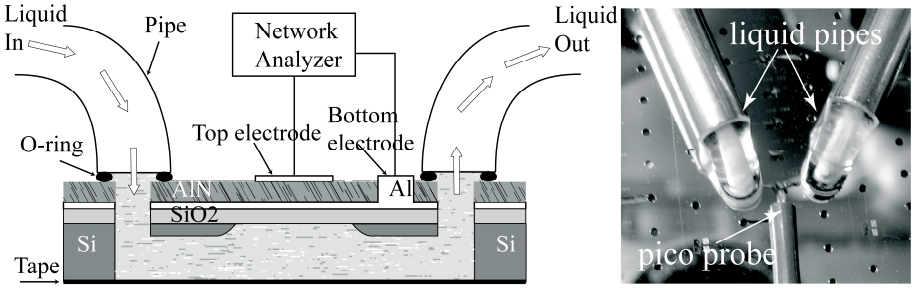

Figure 5.3. (a) Illustration of the measurement setup for in-liquid characterization of the FBARs using a Network Analyzer. (b) Photograph of in-liquid measurement setup.

6 Summary – Main achievements, Comments and Outlook

6.1.1 Main achievements

The author's main contributions to the thin film electroacoustics field are summarized as follows:

1. Development of an original, two step deposition method for the synthesis of piezoelectric AlN thin films with a tilted c-axis for efficient excitation of shear waves in thickness excited FBARs in view of in-liquid operation;
    - easily implemented in a standard sputter deposition system.
    - no additional hardware required.
    - good functional uniformity - k_t^2 of around *2%* over major part of the wafer.

2. Gained knowledge on
    - texture formation from studies of c-axis AlN growth as a function of substrate structure and morphology.
    - spurious mode suppression.

3. Development of AlN Lamb resonators (IDT and LFE);
    - high wave velocity (*>10000 m* s^{-1}).
    - *f = 500-800 MHz,* K_{eff}^2 *= 0.8%.*

4. Development of a practical FBAR design with an integrated micro-fluidic transport system for delivering liquid or gaseous analytes to the FBAR's sensing surface.

5. Design, fabrication and evaluation of temperature compensated shear mode resonators exhibiting;
    - Temperature stability (*TCF = ±2 ppm* $^oC^{-1}$ *for T=25–95* ^oC).
    - high frequency (*1.3 GHz*).
    - high Q in liquid (*230*).
    - sufficient coupling coefficient k_t^2 (*1.4%*).

- mass sensitivity (*~1000 cm^2 g^{-1}*).
- resolution (*better than 2 ng cm^{-2} in liquid*).

Contributions of practical value to the research group at Uppsala University:

1. Assembly of an experimental setup for on-wafer measurements of FBARs including;
    - a microfluidic pumping system for in-liquid measurements.
    - a temperature characterization system for automated temperature measurements.
    - a pressure sensitivity measurement setup.

2. Development of parameter extraction techniques and modeling tools.

6.1.2 Comments, work in progress and outlook

The presented two-stage process for the deposition of tilted AlN films results in a good functional uniformity over the major area of the wafer, which really illustrates the potential of the method since the sputtering system used has in no way been optimized for tilted film synthesis. On the contrary, parameters such as the target-to-substrate distance, magnetron type, shape of target (race track), system geometry, substrate bias, etc. are all fixed for the system used. All this indicates that the process can be further optimized. This is of significant importance for industrial scale fabrication where the requirements on the film properties such as tilt and thickness uniformity, functional uniformity in terms of Q and electromechanical coupling, stress, surface roughness, density as well as deposition rate are extremely stringent. For further reading on the process optimization the reader is referred to [88].

The importance of the seed layer is undisputed and although the underlying mechanisms for tilted film growth have been discussed to some extent in the thesis, definitive proofs for these are yet to be provided. A more rigorous analysis including high resolution TEM studies are currently under way, which are expected to provide a deeper understanding of the process as well as contribute to its further development.

With regard to the development of FBAR based biosensors the results so far have shown to be very promising indeed. Measurements with a network analyzer is a powerful method for on-wafer characterization, which provides data not only of frequency shifts but also information of the damping and loss mechanisms, though, for accurate and reproducible measurements careful calibration as well as a controlled environment are absolutely essential. The setup is sensitive to various sources of disturbances such vibrations, humidity, dust, temperature fluctuations, etc. In order to evaluate the full

potential of these devices, i.e. resolution, such influences should be minimized. An experimental setup for sensor characterization in a clean room environment is under construction.

One of the greatest advantages of the thin film electro-acoustic technology is its natural compatibility with the IC technology as it no longer uses single crystalline materials one the one hand as well as utilizes the planar technology for device fabrication on the other. Thus, the next obvious and natural step is expected to be its monolithic integration with the IC technology which will bring about substantial economic and performance benefits. This is equally true for both telecom and sensor applications. The FBAR sensor technology developed by the author and colleagues at the Thin Film Group at the Ångström laboratory is currently being implemented and further optimized in an EU project (Biognosis) aiming at developing sensor arrays, ultimately monolithically integrated with the associated electronics, for DNA and protein detection in clinical testing and diagnostics [89].

My personal opinion regarding the future of the FBAR technology in biosensor applications is very optimistic. Here I would also include the SMR approach as being a more robust alternative.

Other preliminary studies currently under way in the group concern the use of FBARs as physical and chemical sensors. Initial results on the pressure sensitivity have confirmed our expectations in terms of range and sensitivity.

Another very likely path for the further development of this technology is the synthesis of a wider range of thin piezoelectric films as the properties of the latter determine their suitability for one application or another. Thus for instance, the electromechanical coupling determines the maximum bandwidth of a bandpass filter, which means that in the cases of bandwidths larger than 6% materials with a higher piezoelectric coefficient than that of AlN are needed. In addition, modern telecommunications require electronically configurable solutions which in turn necessitate the use of tunable components such as tunable filters, resonators, oscillators, matching networks, etc. This necessity is already having an impact on the research as efforts are currently being directed towards the synthesis of high performance ferroelectric materials [90, 91].

… in the end – this is only the beginning …

Acknowledgements

It happens that once in a while you must make a life decision. Hesitating and doubtful. Is this the right thing for me? Five years ago I made a choice, now as I'm locking back I know why I started, how I managed and why I succeeded.

.. thank you *Ilia Katardjiev* for your supervision and great support both inside and outside these Ångström walls. I'm looking forward to continuing our teamwork.

I'm happy to belong to the Solid State Electronics' department, not only because of the Friday coffee and buns. It has been almost three years now, since I received flowers and some written words to support me when I needed them the most. I take this opportunity to thank You all and *Sören Berg* who represented the department at that time.

-*Marianne Asplund* you are doing a great job and always with a smile.

-The thin Film group's former members:

Fredrik Engelmark and *Gonzalo Fuentes* thanks for guiding me during my diploma work. Fredrik was also one of those that persuaded me to "Enter the Matrix". I'm glad that I followed your advice.

Daniel Rosén for valuable support and good advises in the clean room.

-The thin Film group's current members:

Gunilla, Johannes, David, Lina, Ventsi. I won't be leaving you yet.

-*Lars Vestling* who co-authored on one of my papers.

-*Jörgen Westlinder,* we where room mates for a period of time, I appreciated our conversations.

Gustaf Sjöblom I've known you since the beginning. You are a good fellow.

-*Jörgen Olsson* for proof-reading this thesis and for the instructions how to master the "Nätverkarn".

-*Björn Kuzavas* for technical support with the experimental setup assemble.

-*Jonas Sundqvist* for a substantial amount of time spent introducing me to the CVD process and XRD measurements.

-*Mikael Ottosson* who taught me how to run the XRD instruments and is the guy you ask for help when all you see on the screen is a straight line.

- *Gunjana Sharma* for the work with channel structures.

- *Zareh Topalian* for the work with WO_3 deposition.

-The MSL force for make things easier for us in the clean room. Special thanks to one of my best friends: – *Anders Heljestrand,* see you in Nallens Leksaker.

- All my other best friends, student colleagues and the Ångström-café-lunch-squad.

- Outside of Ångström, I'm grateful to you all:
"Moster" Angelica, Åsa, familjen Gillespie, LO, Erik E, and Pierre R
"Mormor och morfar", och övriga från södern.

-Min familj:
Pappa
Brorsan m. familj, och övriga från norr.

Slutligen sist och minst, men med en stor personlighet;
Charmtrollet, glädjespridaren, eller kort sagt

Min Son Elias

Johan Bjurström
Februari 2007

Sammanfattning på Svenska

Avancerade elektroakustiska tunnfilms komponenter är ett försök att översätta titeln på denna avhandling. De flesta känner nog till den enormt snabba utveckling som skett inom telekommunikation och annan trådlös dataöverföring. Mobiltelefoner stora som bilbatterier är ett minne blott och har ersatts av dagens små, energisnåla och allt mer avancerade telefoner. Elektroakustiska komponenter, främst frekvensfilter, finns i stort sett i alla moderna telefoner och liknande system som kräver bearbetning av högfrekventa signaler, sk. radiovågor. GSM nätet till exempel använder sig av ett frekvensband runt 1800 MHz för sändning och mottagning av signaler medan WLAN (*Wireless Local Area Network*) använder frekvenser runt 5.2 GHz för dataöverföring. Antalet system ökar hela tiden och en accelererande användning av trådlös kommunikations teknik har lett till att frekvensområdet måste utökas för att möta utvecklingen, vilket har medfört att äldre teknologi måste ersättas av andra lösningar. Elektroakustisk teknologi i kombination med tunnfilmsteknologin gör det möjligt att möta de höga krav som ställs på prestanda, miniatyrisering, låga kostnader, mm. Även fast dessa komponenter funnits kommersiellt sedan början av 2000 talet, har man ännu inte börjat tillverka mikrochip med elektroakustiska komponenter integrerade med IC komponenter vilket skulle minska kostnader och ge möjlighet till ännu mindre, billigare apparater med fler funktioner eller helt nya tillämpningar. De uppenbara fördelarna med en sådan integrering tillsammans med hög prestanda har ändå gjort att komponenter baserade på denna teknologi ökar snabbt i antal och förutspås dominera den framtida marknaden, speciellt för mycket höga frekvenser.

Det har också länge varit känt att elektroakustiska vågor i fasta material och som genereras av elektriska signaler är känsliga för yttre påverkan och kan därför användas i en mängd olika fysikaliska, kemiska och biokemiska sensortillämpningar. Den mest tillämpade egenskapen hos elektroakustiska komponenter, t.ex. resonatorer är deras extrema känslighet för massförändringar på ytan som används för att mäta tunna lager av material som deponeras på ytan. En sådan förändring resulterar i ett litet skift i resonansfrekvensen som är proportionellt mot massändringen.

Tunnfilmsgruppen på Ångströmlaboratoriet i Uppsala har sedan 1997 forskat på att framställa material och komponenter, främst resonatorer, för avancerade elektroakustiska tillämpningar. Forskningen har varit inriktad mot att utveckla en lågtemperaturprocess för att syntetisera tunna filmer (< *5*

μm) av piezoelektrisk aluminiumnitrid (AlN) som är ett av de mest användbara materialen och samtidigt det viktigaste materialet i högfrekventa elektroakustiska komponenter. AlN syntetiseras genom reaktiv sputtring som är en effektiv och flexibel metod där en mängd olika processparametrar kan varieras för att kontrollera AlN filmens egenskaper och kvalité, dvs. hur bra piezoelektriska egenskaper den har, defekter, spänningar, osv. Den viktigaste egenskapen är filmens textur (kristalltillväxtriktning) som under normala förhållanden är c-orienterad. En sådan film uppvisar den starkaste piezoelektriska effekten för pålagt elektriskt fält genom filmen, vinkelrätt mot ytan och är den textur som är mest användbar i filtertillämpningar där ett antal elektroakustiska resonatorer kopplas samman. Det finns en mängd varianter på sådana komponenter och olika vågtyper. Denna avhandling fokuserar i huvudsak på vågor som propagerar i tjockleksriktningen genom filmen och är i fallet för c-orienterade filmer longitudinella vågor, dvs. tryckvågor. En annan typ av våg som propagerar parallellt med ytan i ett tunt membran, sk. lambvågor, har också studerats.

Mitt bidrag till forskningen – Arbetet var inledningsvis fokuserat på att karaktärisera och utvärdera AlN processen för att samla kunskap om bakomliggande faktorer som styr filmtillväxt och textur vilket har stor betydelse för kvalitén och prestanda hos komponenterna. De första komponenterna som tillverkades var tunnfilmsresonatorer eller FBARs (Film Bulk Acoustic Resonators) och användes för att elektroakustiskt utvärdera AlN filmen. Den uppmätta prestandan kan uttryckas i termer som elektromekanisk kopplingskoefficient och Q-värde där den första beskriver hur effektiv konverteringen mellan elektrisk och mekanisk energi är medan Q-värdet är ett mått på hur stora förluster (akustiska och elektriska) resonatorn har och där lågt Q motsvarar stora förluster. Sådana egenskaper beror inte enbart på materialet den är gjord av utan också på hur resonatorn är designad. De första artiklarna i denna avhandling är resultat från detta inledande arbete. Metoder för snabb och effektiv utvärdering av AlN film egenskaper utvecklades (artikel I), olika resonator topologier studerades (artikel II), samt en stor del av arbetet gav en grundläggande förståelse för AlN filmtillväxt och hur olika processparametrar inverkar på texturen (artiklar III-IV).

Det absolut mest betydelsefulla resultatet med min forskning som jag presenterar i denna avhandling var arbetet med att utveckla en metod för sputter deponering av AlN filmer med tiltad kristalltextur, dvs. c-riktningen är i detta fall inte vinkelrät mot ytan utan lutar ca 30º. Det betyder att även transversella vågor kan skapas i AlN filmen med relativt hög koppling (~2%). Möjligheten att använda den transversella vågen har öppnat upp ett helt nytt forskningsområde för tunnfilmsbaserade komponenter där möjligheten finns att mäta massförändringar i vätskor med stor noggrannhet och dessutom studera vätskornas egenskaper. Denna teknik har funnits många år men den största skillnaden är att tunnfilmsbaserade resonatorer arbetar vid mycket

högre frekvenser som enligt teorin har en många gånger högre känslighet. Denna process som också resulterade i ett patent finns beskriven i detalj i artikel V. Resultat från mätningar i vätska på tunnfilmsresonatorer som använder den transversella vågen har inte bara visat hög känslighet utan också höga Q värden, dvs. låga förluster till den omgivande vätskan. Detta i sin tur betyder att upplösningen, den minsta detekterbara massförändringen, med en sådan sensor förväntas vara mycket bra och har redan visat sig vara i nivå med eller bättre än existerande liknande metoder (<2 ng/cm^2). Ett stort tillämpningsområde är det medicinska, där elektroakustiska resonatorer kan användas som biosensorer för detektion av små mängder biomaterial i för olika syften, t.ex. cancerdiagnostik, mm. För att ytterligare förbättra upplösning och temperatur stabiliteten designades och tillverkades en variant av resonatorn som i stort sett var temperaturoberoende i området 25-95ºC och samtidigt uppvisade högt Q (~200) och bra kopplingkoefficient i vätska (se artikel IX). Parallellt med detta arbete har andra typer av resonatorer studerats med egenskaper som är användbara för högfrekvenstillämpningar. Speciellt, en typ av tunnfilmsresonator där den elektroakustiska vågen propagerar inuti ett membran parallellt med ytan har visat sig lovande. Sådana vågor (Lamb-vågor) kan uppnå mycket höga våghastigheter och samtidigt höga Q värden vilket alltid är önskvärt i denna typ av komponenter, se artiklar VI, VII.

Summary of Appended Papers

Paper I

"An accurate direct extraction technique for the MBVD resonator model"

Paper I describes a quick extraction method of the six elements in the MBVD model directly from S_{11} measurements. The method is easily implemented in a MATLAB (or equivalent software) program and used as a function incorporated in a computer controlled data acquisition system including:

1. Measuring S_{11} (1601 points),
2. S_{11} data transfer from the NWA to the computer,
3. S_{11} to Y (admittance) conversion,
4. parameter extraction (the proposed method) and finally,
5. result presentation or parameter storage.

Paper II

"Suppression of Spurious Lateral Modes in Thickness-Excited FBAR Resonators"

This work explores the apodization method for suppressing spurious effects caused by lateral-excited modes by studying their dependence on the electrode geometry. The origin of the lateral-excited modes is discussed in some detail, and the results from different electrode geometries are compared. A new elliptical electrode shape for suppression of spurious modes is developed and demonstrated.

It is confirmed that resonators with parallel electrode edges exhibit a substantial spurious response due to lateral-mode constructive interference. It is demonstrated that resonators with an elliptical electrode or irregular shape smooth out the frequency response.

Paper III

"Synthesis of C-Axis-Oriented AlN Thin Films on High-Conducting Layers: Al, Mo, Ti, TiN, and Ni"

The aim of the work in Paper III was primarily to identify which factors and properties of the underlying layer determine the AlN texture.

The results show a direct correlation between the degree of texture of the underlying film with that of the AlN film. In addition, the AlN texture worsens with increasing surface roughness. An interesting observation is that a smooth substrate surface does not automatically generate high textured AlN films. The results illustrate the need of both well-textured and smooth surfaces in order to grow oriented films. Under these conditions a good lattice match both in terms of symmetry and lattice parameter between the substrate surface plane and the AlN (002) plane is equally important for highly textured growth. This conclusion is confirmed by the observation that the texture of AlN films grown onto Ti (002) surfaces is better than that of films grown onto Al (111) crystallographic surfaces.

Paper IV

"Dependence of the Electromechanical Coupling on the Degree of Orientation of c-Textured Thin AlN Films"

The goal of this work is to study the variation of the electromechanical coupling and the quality factor of the resonators, for both the longitudinal and the shear modes as a function of the degree of film texture. It is observed that the films exhibit a mean tilt of the c-axis relative to the surface normal. This tilt is found to depend on both the film texture and the distance from the wafer radius. It is also demonstrated that the textured films exhibit a behavior of the electromechanical coupling effectively identical to that of a single crystalline material of an equivalent tilt. Thus, it is shown that the electromechanical coupling for the longitudinal mode decreases from 8% to 4%, and that for the shear mode increases from 0% up to 3% by varying the full width half maximum (FWHM) of the (002) rocking curve in the interval from 2º to 10º.

Paper V

"Synthesis of Textured Thin Piezoelectric AlN Films With a Nonzero C-Axis Mean Tilt for the Fabrication of Shear Mode Resonators"

A unique method for the deposition of thin piezoelectric aluminum nitride (AlN) films with a nonzero c-axis mean tilt has been developed. The deposition is done in a standard reactive magnetron sputter deposition system without any hardware modifications.

The resulting films have a distinct tilted texture with a mean tilt of the c-axis varying roughly in the interval *28 to 32* degrees over the radius of the wafer excluding a small exclusion zone at the center of the latter. The shear mode resonance frequency was about *1.6 GHz,* the extracted device *Q* around *350*, and the electromechanical coupling k_2^t *2%* when the resonator was operated in air, whereas the latter two dropped down to 150 and 1.8%, respectively, when the resonator was operated in pure water.

Paper VI

"Lateral-field-excited thin-film Lamb wave resonator"

The basic principles and technology for the development of lateral-field-excited Lamb acoustic wave resonators on sputter-deposited c-oriented thin aluminum nitride films are presented. Various Lamb wave resonators are designed and fabricated.

It is shown that the first symmetric Lamb mode exhibits a very high velocity of propagation of around 10 300 m/s at resonance frequency, the device Q is 880 yielding a figure of merit $Qxf = 0.5\ 10^{12}\ s^{-1}$. The effective device coupling is $K_{eff}^2 = 0.8\%$.

Paper VII

"Thin film Lamb wave resonant structures – The first approach"

Resonant Lamb wave based geometries on c-oriented aluminum nitride (AlN) thin film membranes are studied. Attention has been focused on the lowest order symmetric Lamb mode because of its extremely high velocity approaching 10,600 m/s. The Lamb waves have been excited by means of both inter-digital transducers (IDT) and longitudinal wave (LW) transducers. Two basic reflector geometries have been used along with the conventional one-port resonator topology.

The excitation efficiency of the LW excited devices is found to be around 0.8% while that of the IDT excited devices of the order of 0.4% for a frequency range, *f =500-800MHz.*

Paper VIII

"Shear mode AlN thin film electro-acoustic resonant sensor operation in viscous media"

A shear mode thin film bulk acoustic resonator (FBAR) operating in liquid media together with a microfluidic transport system is presented. The resonator has been fabricated utilizing a recently developed reactive sputter-deposition process for AlN thin films with inclined c-axis relative to the surface normal with a mean tilt of around 30º. Sensor operation in water and glycerol solutions is characterized. Theoretical analysis of the sensor operation under viscous load as well as of the sensitivity and stability in general is presented.

The results illustrate clearly that the tilted thin film electro-acoustic sensor technology represents a competitive alternative to the single crystal QCM technology, since it is characterized with extreme sensitivity, higher resolution, small size, low cost and is compatible with the standard IC technology. The mass resolution demonstrated even in a non-controlled environment excels that of QCM.

Paper IX

"Temperature compensation of liquid FBAR sensors"

The paper studies intrinsic temperature compensation of FBARs and deals with the design, fabrication and characterization of a temperature compensated Al/AlN/Al/SiO_2 composite FBAR. The aim was to enhance the performance of the FBAR as a liquid sensor in terms of improved thermal stability, increased resonator Q in liquids at the expense of a minimal loss in coupling coefficient. The resonators evaluated have an AlN thickness of around 2 μm, 200 nm top and bottom Al electrodes while the SiO_2 thickness was varied in the range 1.0 to 1.55 μm. The substrate temperature was ramped in steps of 10ºC in the interval 25ºC to 95ºC using a probe station equipped with a Thermochuck (model TP0315A, Temptronic Corporation).

Figure 1 shows the calculated TCF (at room temperature) for both predicted and measured resonance frequencies for the first and second harmonic longitudinal and shear mode as a function of the SiO_2 thickness. A practically complete temperature compensation is achieved for the second harmonic shear mode which also exhibits an excellent Q (*230*) and high coupling coefficient (*1.4%*) in pure water.

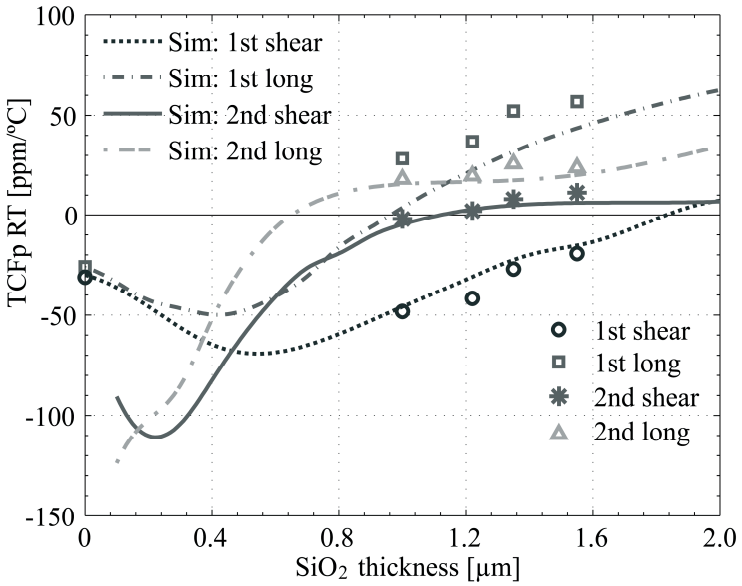

Figure 1. Calculated and measured TCF (at room temperature) for both the first and the second harmonic shear and longitudinal mode as a function of the SiO_2 thickness.

References

[1] A. Ballato, "Piezoelectricity: history and new thrusts," *IEEE Ultrasonics Symposium Proceedings*, vol. 1, pp. 575-583 vol.1, 1996.

[2] R. Weigel, D. P. Morgan, J. M. Owens, A. Ballato, K. M. Lakin, K. Hashimoto, and C. C. W. Ruppel, "Microwave acoustic materials, devices, and applications," *Microwave Theory and Techniques, IEEE Transactions on*, vol. 50, pp. 738-749, 2002.

[3] R. Aigner, "MEMS in RF Filter Applications: Thin-film Bulk Acoustic Wave Technology," *Sensors Update*, vol. 12, pp. 175-210, 2003.

[4] K. M. Lakin, "Thin film resonator technology," *Ultrasonics, Ferroelectrics and Frequency Control, IEEE Transactions on*, vol. 52, pp. 707-716, 2005.

[5] N. F. Foster, "Ultra-high frequency cadmium-sulphide transducers," *IEEE Transactions on Sonics and Ultrasonics*, vol. SU-11, pp. 63-68, 1964.

[6] T. R. Sliker and D. A. Roberts, "A Thin-Film CdS-Quartz Composite Resonator," *Journal of Applied Physics*, vol. 38, pp. 2350-2358, 1967.

[7] T. Shiosaki, T. Yamamoto, T. Oda, and A. Kawabata, "Low-temperature growth of piezoelectric AlN film by RF reactive planar magnetron sputtering," *Applied Physics Letters*, vol. 36, pp. 643-5, 1980.

[8] J. S. Wang and K. M. Lakin, "Sputtered AlN Films for Bulk-Acoustic-Wave Devices," *IEEE Ultrasonics Symposium Proceedings*, pp. 502-505, 1981.

[9] R. Ruby and P. Merchant, "Micromachined thin film bulk acoustic resonators," *IEEE International Frequency Control Symposium Proceedings*, pp. 135-138, 1994.

[10] K. M. Lakin, G. R. Kline, and K. T. McCarron, "Thin film bulk acoustic wave filters for GPS," *IEEE Ultrasonics Symposium Proceedings*, pp. 471-6, 1992.

[11] D. McNamara, "FBAR technology shrinks CDMA handset duplexers," *Microwaves & RF*, vol. 39, pp. 71-9, 2000.

[12] R. C. Ruby, P. Bradley, Y. Oshmyansky, A. Chien, and J. D. Larson Iii, "Thin film bulk wave acoustic resonators (FBAR) for wireless applications," *IEEE Ultrasonics Symposium Proceedings*, vol. 1, pp. 813-821, 2001.

[13] V. Yantchev and I. Katardjiev, "Micromachined thin film plate acoustic resonators utilizing the lowest order symmetric lamb wave mode," *Ultrasonics, Ferroelectrics and Frequency Control, IEEE Transactions on*, vol. 54, pp. 87-95, 2007.

[14] G. G. Fattinger, J. Kaitila, R. Aigner, and W. Nessler, "Thin film bulk acoustic wave devices for applications at 5.2 GHz," *IEEE Ultrasonics Symposium Proceedings*, vol. 1, pp. 174-177 Vol.1, 2003.

[15] W. A. Burkland, A. R. Landin, G. R. Kline, and R. S. Ketcham, "A thin-film bulk-acoustic-wave resonator-controlled oscillator on silicon," *Electron Device Letters, IEEE*, vol. 8, pp. 531-533, 1987.

[16] S. G. Burns, R. J. Weber, and S. D. Braymen, "High frequency oscillators using cointegrated BAW thin-film piezoelectrics with microwave BJTs," *Frequency Control, Proceedings of the 45th Annual Symposium on*, pp. 207-211, 1991.

[17] B. Drafts, "Acoustic wave technology sensors," *Microwave Theory and Techniques, IEEE Transactions on*, vol. 49, pp. 795-802, 2001.

[18] F. Herrmann, B. Jakoby, J. Rabe, and S. Büttgenbach, "Microacoustic Sensors for Liquid Monitoring," *Sensors Update*, vol. 9, pp. 105-160, 2001.

[19] G. Wingqvist, J. Bjurstrom, L. Liljeholm, I. Katardjiev, and A. L. Spetz, "Shear mode AlN thin film electroacoustic resonator for biosensor applications," presented at IEEE Sensors, Irvine, CA, USA, 2005.

[20] R. Gabl, H. D. Feucht, H. Zeininger, G. Eckstein, M. Schreiter, R. Primig, D. Pitzer, and W. Wersing, "First results on label-free detection of DNA and protein molecules using a novel integrated sensor technology based on gravimetric detection principles," *Biosensors and Bioelectronics*, vol. 19, pp. 615-620, 2004.

[21] S. Rey-Mermet, R. Lanz, and P. Muralt, "Bulk acoustic wave resonator operating at 8 GHz for gravimetric sensing of organic films," *Sensors and Actuators B: Chemical*, vol. 114, pp. 681-686, 2006.

[22] H. Zhang and E. S. Kim, "Micromachined acoustic resonant mass sensor," *Journal of Microelectromechanical Systems*, vol. 14, pp. 699-706, 2005.

[23] J. Weber, W. M. Albers, J. Tuppurainen, M. Link, R. Gabl, W. Wersing, and M. Schreiter, "Shear mode FBARs as highly sensitive liquid biosensors," *Sensors and Actuators A: Physical*, vol. 128, pp. 84-88, 2006.

[24] J. F. Rosenbaum, *Bulk Acoustic Wave Theory and Devices*: Artech House, 1988.

[25] D. S. Ballantine, R. M. White, S. J. Martin, A. J. Ricco, E. T. Zellers, G. C. Frye, and H. Wohltjen, *Acoustic wave sensors; theory, design, and physico - chemical applications*: Academic Press, 1997.

[26] R. M. White and F. W. Voltmer, "Direct piezoelectric coupling to surface elastic waves " *Applied Physics Letters*, vol. 7, pp. 314-316, 1965.

[27] K. M. Lakin, J. Belsick, J. F. McDonald, and K. T. McCarron, "Improved bulk wave resonator coupling coefficient for wide bandwidth filters," *IEEE Ultrasonics Symposium Proceedings*, vol. vol.1, pp. 827-31, 2001.

[28] K. Tsubouchi, K. Sugai, and N. Mikoshiba, "AlN Material Constants Evaluation and SAW Properties on AlN/Al_2O_3 and AlN/Si," *IEEE Ultrasonics Symposium Proceedings*, pp. 375-380, 1981.

[29] G. F. Iriarte, "AlN thin film electroacoustic devices," Ph. Doctoral Thesis,Uppsala University, 2003, pp. 67.

[30] R. S. Naik, R. Reif, J. J. Lutsky, and C. G. Sodini, "Low-temperature deposition of highly textured aluminum nitride by direct current magnetron sputtering for applications in thin-film resonators," *Journal of the Electrochemical Society*, vol. 146, pp. 691-696, 1999.

[31] F. Engelmark, "AlN and high-*k* thin films for IC and electroacoustic applications," Ph. Doctoral Thesis, Uppsala University, 2002, pp. 80.

[32] G. F. Iriarte, F. Engelmark, and I. V. Katardjiev, "Reactive sputter deposition of highly oriented AlN films at room temperature," *Journal of Materials Research*, vol. 17, pp. 1469-75, 2002.

[33] G. F. Iriarte, F. Engelmark, M. Ottosson, and I. V. Katardjiev, "Influence of deposition parameters on the stress of magnetron sputter-deposited AlN thin films on Si(100) substrates," *Journal of Materials Research*, vol. 18, pp. 423-32, 2003.

[34] Y. Kajikawa, S. Noda, and H. Komiyama, "Comprehensive perspective on the mechanism of preferred orientation in reactive-sputter-deposited nitrides," *Journal of Vacuum Science and Technology A: Vacuum, Surfaces and Films*, vol. 21, pp. 1943-1954, 2003.

[35] J. K. Liu, K. M. Lakin, and K. L. Wang, "Growth morphology and surface-acoustic-wave measurements of AlN films on sapphire," *Journal of Applied Physics*, vol. 46, pp. 3703-6, 1975.

[36] H. P. Loebl, M. Klee, C. Metzmacher, W. Brand, R. Milsom, and P. Lok, "Piezoelectric thin AlN films for bulk acoustic wave (BAW) resonators," *Materials Chemistry and Physics*, vol. 79, pp. 143-146, 2003.

[37] W. T. Lim, B. K. Son, D. H. Kang, and C. H. Lee, "Structural properties of AlN films grown on Si, Ru/Si and ZnO/Si substrates," *Thin Solid Films*, vol. 382, pp. 56-60, 2001.

[38] H. P. Lobl, M. Klee, O. Wunnicke, R. Kiewitt, R. Dekker, and E. V. Pelt, "Piezo-electric AlN and PZT films for micro-electronic applications," *IEEE Ultrasonics Symposium Proceedings*, vol. vol.2, pp. 1031-6, 1999.

[39] D. Marc-Alexandre and M. Paul, "Properties of aluminum nitride thin films for piezoelectric transducers and microwave filter applications," *Applied Physics Letters*, vol. 74, pp. 3032-3034, 1999.

[40] M.-A. Dubois and P. Muralt, "Measurement of the effective transverse piezoelectric coefficient $e_{31,f}$ of AlN and $Pb(Zr_x,Ti_{1-x})O_3$ thin films," *Sensors and Actuators, A: Physical*, vol. 77, pp. 106-112, 1999.

[41] M. A. Dubois, P. Muralt, H. Matsumoto, and V. Plessky, "Solidly mounted resonator based on aluminum nitride thin film," *IEEE Ultrasonics Symposium Proceedings*, vol. vol.1, pp. 909-12, 1998.

[42] F. S. Hickernell, "Measurement techniques for evaluating piezoelectric thin films," *IEEE Ultrasonics Symposium Proceedings*, vol. vol.1, pp. 235-42, 1996.

[43] A. L. Kholkin, W. Ch, D. V. Taylor, and N. Setter, "Interferometric measurements of electric field-induced displacements in piezoelectric thin films," *Review of Scientific Instruments*, vol. 67, pp. 1935-1941, 1996.

[44] R. S. Naik, J. J. Lutsky, R. Reif, C. G. Sodini, A. Becker, L. Fetter, H. Huggins, R. Miller, J. Pastalan, G. Rittenhouse, and Y. H. Wong, "Measurements of the bulk, C-axis electromechanical coupling constant as a function of AlN film quality," *Ultrasonics, Ferroelectrics and Frequency Control, IEEE Transactions on*, vol. 47, pp. 292-296, 2000.

[45] J. A. Ruffner, P. G. Clem, B. A. Tuttle, D. Dimos, and D. M. Gonzales, "Effect of substrate composition on the piezoelectric response of reactively sputtered AlN thin films," *Thin Solid Films*, vol. 354, pp. 256-261, 1999.

[46] R. Thalhammer, J. Kaitila, R. Aigner, and S. Marksteiner, "Prediction of BAW resonator performance using experimental and numerical methods," *IEEE Ultrasonics Symposium Proceedings*, vol. 1, pp. 282-285 Vol.1, 2004.

[47] T. Makkonen, A. Holappa, J. Ella, and M. M. Salomea, "Finite element simulations of thin-film composite BAW resonators," *Ultrasonics, Ferroelectrics and Frequency Control, IEEE Transactions on*, vol. 48, pp. 1241-1258, 2001.

[48] J. E. Graebner, H. F. Safar, B. Barber, P. L. Gammel, G. J. Herbsommer, L. A. Fetter, J. Pastalan, H. A. Huggins, and R. E. Miller, "Optical mapping of surface vibrations on a thin-film resonator near 2 GHz," *IEEE Ultrasonics Symposium Proceedings*, vol. vol.1, pp. 635-8, 2000.

[49] R. C. Ruby, J. D. Larson, R. S. Fazzio, and C. Feng, "Performance degradation effects in FBAR filters and resonators due to lamb wave modes," *IEEE Ultrasonics Symposium Proceedings*, vol. 3, pp. 1832-1835, 2005.

[50] G. G. Fattinger, M. R. Fattinger, K. Diefenbeck, P. Muller, and R. Aigner, "Spurious mode suppression in coupled resonator filters," *IEEE Microwave Symposium Digest MTT-S International*, pp. 4 pp., 2005.

[51] N. F. Foster, "Performance of Shear Mode Zinc Oxide Thin-Film Ultrasonic Transducers," *Journal of Applied Physics*, vol. 40, pp. 4202-4204, 1969.

[52] M. Minakata, N. Chubachi, and Y. Kikuchi, "Variation of c-axis orientation of ZnO thin films deposited by DC sputtering," *Jap. J. Appl. Phys.*, vol. 12, pp. 474-475, 1973.

[53] J. S. Wang, K. M. Lakin, and A. R. Landin, "Sputtered C-Axis Inclined Piezoelectric Films and Shear Wave Resonators," *Frequency Control, 37th Annual Symposium* pp. 144-150, 1983.

[54] S. V. Krishnaswamy, B. R. McAvoy, W. J. Takei, and R. A. Moore, "Oriented ZnO Films for Microwave Shear Mode Transducers," *IEEE Ultrasonics Symposium Proceedings*, pp. 476-479, 1982.

[55] H. Nowotny and E. Benes, "General one-dimensional treatment of the layered piezoelectric resonator with two electrodes," *Journal of the Acoustical Society of America*, vol. 82, pp. 513-21, 1987.

[56] H. M. Liaw and F. S. Hickernell, "The characterization of sputtered polycrystalline aluminum nitride on silicon by surface acoustic wave measurements," *Ultrasonics, Ferroelectrics and Frequency Control, IEEE Transactions on*, vol. 42, pp. 404-409, 1995.

[57] A. Ballato and J. G. Gualtieri, "Advances in high-Q piezoelectric resonator materials and devices," *Ultrasonics, Ferroelectrics and Frequency Control, IEEE Transactions on*, vol. 41, pp. 834-844, 1994.

[58] N. Oura, N. Kuramochi, M. Koshino, and T. Katsumoto, "Defects in synthetic quartz and the Q-values of the -18.5° X-cut bar " *Japanese Journal of Applied Physics*, vol. 20, pp. 157-160, 1981.

[59] J. B. Lee, S. H. Kwak, and H. J. Kim, "Effects of surface roughness of substrates on the c-axis preferred orientation of ZnO films deposited by r.f. magnetron sputtering," *Thin Solid Films*, vol. 423, pp. 262-266, 2003.

[60] S. H. Lee, J. H. Kim, G. D. Mansfeld, K. H. Yoon, and J. K. Lee, "Influence of electrodes and Bragg reflector on the quality of thin film bulk acoustic wave resonators," *IEEE Frequency Control Symposium and PDA Exhibition*, pp. 45-49, 2002.

[61] R. Ruby, J. Larson, C. Feng, and S. Fazzio, "The effect of perimeter geometry on FBAR resonator electrical performance," *Microwave Symposium Digest IEEE MTT-S International*, pp. 4 pp., 2005.

[62] "IEEE standard on piezoelectricity," Inst. Electr. & Electron. Eng., New York, NY, USA, Copyright 1988, IEE ANSI/IEEE Std 176-1987, 1988.

[63] K. M. Lakin, G. R. Kline, and K. T. McCarron, "High-Q microwave acoustic resonators and filters," *Microwave Theory and Techniques, IEEE Transactions on*, vol. 41, pp. 2139-2146, 1993.

[64] J. D. Larson III, P. D. Bradley, S. Wartenberg, and R. C. Ruby, "Modified Butterworth-Van Dyke circuit for FBAR resonators and automated measurement system," *IEEE Ultrasonics Symposium Proceedings*, vol. 1, pp. 863-868, 2000.

[65] M.-C. Chao, Z.-N. Huang, S.-Y. Pao, Z. Wang, and C. S. Lam, "Modified BVD-equivalent circuit of FBAR by taking electrodes into account," *IEEE Ultrasonics Symposium Proceedings*, vol. 1, pp. 973-976, 2002.

[66] L. Vestling and J. Ankarcrona, "A general small-signal series impedance extraction technique," *Microwave and Wireless Components Letters, IEEE*, vol. 12, pp. 249-251, 2002.

[67] J. Enlund, I. Katardjiev, and D. M. Martin, "Fabrication and evaluation of an "electrodeless" solidly mounted thin film electroacoustic resonator," *IEEE Ultrasonics Symposium Proceedings*, vol. 3, pp. 1837-1839, 2005.

[68] D. E. Pierce, K. Yoonkee, and J. R. Vig, "A temperature insensitive quartz microbalance," *Ultrasonics, Ferroelectrics and Frequency Control, IEEE Transactions on*, vol. 45, pp. 1238-1245, 1998.

[69] K. M. Lakin, K. T. McCarron, and J. F. McDonald, "Temperature compensated bulk acoustic thin film resonators," *IEEE Ultrasonics Symposium Proceedings*, vol. 1, pp. 855-858, 2000.

[70] K. Yamanouchi and S. Hayama, "SAW Properties of SiO_2/128^o Y-X $LiNb0_3$ Structure Fabricated by Magnetron Sputtering Technique," *Sonics and Ultrasonics, IEEE Transactions on*, vol. 31, pp. 51-57, 1984.

[71] P. Wu, N. W. Emanetoglu, X. Tong, and Y. Lu, "Temperature compensation of SAW in ZnO/SiO_2/Si structure," *IEEE Ultrasonics Symposium Proceedings*, vol. 1, pp. 211-214 vol.1, 2001.

[72] Y. Hongyu, P. Wei, Z. Hao, and K. Eun Sok, "Film bulk acoustic resonator at 4.4 GHz with ultra low temperature coefficient of resonant frequency," *18th IEEE International Conference on Micro Electro Mechanical Systems*, pp. 28-31, 2005.

[73] Y. Miyasaka, S. Hoshino, and S. Takahashi, "Advances in structure and fabrication process for thin film acoustic resonator," *IEEE Ultrasonics Symposium Proceedings*, pp. 385-393, 1987.

[74] K. M. Lakin and J. S. Wang, "Acoustic bulk wave composite resonators," *Applied Physics Letters*, vol. 38, pp. 125-127, 1981.

[75] A. Link, E. Schmidhammer, H. Heinze, M. Mayer, M. Schmiedgen, B. Bader, K. Wagner, and R. Weigel, "Suppression of spurious modes in mirror-type thin film BAW resonators using an appropriate shape of the active area," *IEEE Ultrasonics Symposium Proceedings*, vol. 2, pp. 1179-1182, 2005.

[76] J. D. Larson, R. Ruby, and P. Bradley, "Bulk acoustic wave resonator with improved lateral mode suppression," *U.S. Patent 6215375*, 2001.

[77] H. Nakahata, A. Hachigo, K. Higaki, S. Fujii, S. Shikata, and N. Fujimori, "Theoretical study on SAW characteristics of layered structures including a diamond layer," *Ultrasonics, Ferroelectrics and Frequency Control, IEEE Transactions on*, vol. 42, pp. 362-375, 1995.

[78] G. F. Iriarte, F. Engelmark, I. V. Katardjiev, V. Plessky, and V. Yantchev, "SAW COM-parameter extraction in AlN/diamond layered structures," *Ultrasonics, Ferroelectrics and Frequency Control, IEEE Transactions on*, vol. 50, pp. 1542-1547, 2003.

[79] R. Duhamel, L. Robert, H. Jia, F. Li, F. Lardet-Vieudrin, J. F. Manceau, and F. Bastien, "Sensitivity of a Lamb wave sensor with 2 μm AlN membrane," *Ultrasonics*, vol. 44, pp. 893-897, 2006.

[80] S. G. Joshi and Y. Jin, "Excitation of ultrasonic Lamb waves in piezoelectric plates," *Journal of Applied Physics*, vol. 69, pp. 8018-8024, 1991.

[81] M. Pappalardo, "Stiffness-controlled variable-acoustic-delay line," *Applied Physics Letters*, vol. 37, pp. 893-895, 1980.

[82] D. M. Martin, V. Yantchev, and I. Katardjiev, "Buried electrode electroacoustic technology for the fabrication of thin film based resonant components," *Journal of Micromechanics and Microengineering*, vol. 16, pp. 1869-74, 2006.

[83] J. R. Vig and F. L. Walls, "A review of sensor sensitivity and stability," *IEEE/EIA International Frequency Control Symposium and Exhibition Proceedings*, pp. 30-33, 2000.

[84] "IEEE standard definitions of physical quantities for fundamental frequency and time metrology - random instabilities," *IEEE Std 1139-1999*, 1999.

[85] K. K. Kanazawa and J. G. Gordon, "Frequency of a quartz microbalance in contact with liquid," *Anal. Chem.*, vol. 57, pp. 1770-1771, 1985.

[86] S. J. Martin, G. C. Frye, A. J. Ricco, and S. D. Senturia, "Effect of surface roughness on the response of thickness-shear mode resonators in liquids," *Anal. Chem.*, vol. 65, pp. 2910-2922, 1993.

[87] G. Wingqvist, J. Bjurstrom, A.-C. Hellgren, and I. Katardjiev, "Immunosensor utilizing Shear mode thin film bulk acoustic sensor," presented at 20th Anniversary Eurosensors Göteborg, Sweden, 2006.

[88] I. Katardjiev, J. Bjurström, and G. Wingqvist, "Production of polycrystalline films for shear mode piezoelectric thin film resonators ", International patent application PCT/SE2006/050041, 2006 ed. Sweden, 2006.

[89] Biognosis, "Integrated Biosensor System for Label-Free In-Vitro DNA and Protein Diagnostics in Health-Care Applications (BIOGNOSIS) http://cordis.europa.eu/fetch?CALLER=PROJ_IST&ACTION=D&RCN=74650&DOC=330&CAT=PROJ&QUERY=1."

[90] C. Choong-Rae, K. Ilia, G. Michael, and G. Alex, "$Na_{0.5}K_{0.5}NbO_3$ thin films for voltage controlled acoustoelectric device applications," *Applied Physics Letters*, vol. 80, pp. 3171-3173, 2002.

[91] S. Gevorgian, T. Lewin, H. Jacobsson, and A. Vorbiev, "Tuneable Bulk Acoustic Resonator (TFBAR)," Ericsson AB application P19309WO1, 2004 PCT/SE2004/001099 ed, July 2004.

Acta Universitatis Upsaliensis

Digital Comprehensive Summaries of Uppsala Dissertations from the Faculty of Science and Technology 280

Editor: The Dean of the Faculty of Science and Technology

A doctoral dissertation from the Faculty of Science and Technology, Uppsala University, is usually a summary of a number of papers. A few copies of the complete dissertation are kept at major Swedish research libraries, while the summary alone is distributed internationally through the series Digital Comprehensive Summaries of Uppsala Dissertations from the Faculty of Science and Technology. (Prior to January, 2005, the series was published under the title "Comprehensive Summaries of Uppsala Dissertations from the Faculty of Science and Technology".)

Distribution: publications.uu.se
urn:nbn:se:uu:diva-7672

ACTA
UNIVERSITATIS
UPSALIENSIS
UPPSALA
2007